Deuterium spectroscopy for enhanced bounds on physics beyond the standard model

Robert M. Potvliege ⬤,* Adair Nicolson ⬤,† and Matthew P. A. Jones ⬤‡
Department of Physics, Durham University, South Road, Durham DH1 3LE, United Kingdom

Michael Spannowsky ⬤§
Department of Physics, Institute of Particle Physics Phenomenology, Durham University, South Road, Durham DH1 3LE, United Kingdom

We consider the impact of combining precision spectroscopic measurements made in atomic hydrogen with similar measurements made in atomic deuterium on the search for physics beyond the standard model. Specifically, we consider the wide class of models that can be described by an effective Yukawa-type interaction between the nucleus and the electron. We find that it is possible to set bounds on new light-mass bosons that are orders of magnitude more sensitive than those set using a single isotope only, provided the interaction couples differently to the deuteron and proton. Further enhancements of these bounds by an order of magnitude or more would be made possible by extending the current measurements of the isotope shift of the $1s_{1/2}$-$2s_{1/2}$ transition frequency to that of a transition between the $2s_{1/2}$ state and a Rydberg s state.

I. INTRODUCTION

The exquisite precision now achievable in optical frequency measurements and the ongoing development of methods for cooling and trapping atoms, molecules, and highly charged ions suscitate a growing interest in searching for new physics beyond the standard model using precision spectroscopy [1–8]. Spectroscopy experiments already complement existing measurement strategies from high-energy physics experiments and astrophysical observations [9].

However, one of the biggest challenges to fully exploiting the measurement precision currently achievable is the difficulty of direct comparison with the predictions of the standard model for many-electron atoms. The achievable precision in calculations of transition frequencies for these systems is limited by the difficulty of exactly solving the many-electron Schrödinger equation to the required level of accuracy and, more fundamentally, by a lack of knowledge about the necessary many-electron quantum electrodynamics (QED) corrections.

Two approaches around this problem have been proposed. The first is based on many-electron atoms but reduces the need for precise electronic structure calculations by considering different isotopes of the same species [10–12]. Since it was first proposed, this method has been applied to experiments in trapped ions [13–16]. However, the identification of physics beyond the standard model in this approach is complicated by computational difficulties [17] and by the need to use sufficiently accurate models of the nuclei considered [18–20].

The other approach is to use hydrogenic atoms, for which the necessary QED calculations can often be done to a precision matching the experimental error on the measured transitions. Early work in this direction extended the isotope shift method to isotopes of hydrogen and helium [6]. Subsequently, our group showed that direct-experiment theory comparison across an entire set of spectroscopic data (in this case for ^{1}H) could be used to set global bounds on beyond standard model forces [7]. This approach was recently significantly extended by Delaunay *et al.*, who performed a global fit to the entire set of relevant Committee on Data for Science and Technology (CODATA) measurements (not just hydrogenlike atoms) [8].

In this paper we use both the isotope shift and global constraint approaches to set new bounds using spectroscopic measurements in the electronic and muonic isotopes of hydrogen only. Measurements in ordinary hydrogen set a bound on the product of the constants g_e and g_p parametrizing how the electron and the proton, respectively, couple to a hypothetical new physics (NP) boson. The presence of a neutron in the deuterium nucleus introduces a different product of coupling constants for this species, i.e., $g_e g_d$ rather than $g_e g_p$. It is reasonable to assume that g_d differs significantly from g_p. For example, it has been noted that the beryllium anomaly [21,22] can be explained by a light NP boson with a mass of approximately 17 MeV that couples potentially very differently to protons and neutrons [23,24]. We find that the overall bound on possible fifth forces is extremely sensitive to the ratio g_d/g_p

---

*r.m.potvliege@durham.ac.uk

†Present address: UCL Department of Chemistry, University College London, 20 Gordon Street, Kings Cross, London WC1E 6BT, United Kingdom.

‡m.p.a.jones@durham.ac.uk

§michael.spannowsky@durham.ac.uk

with the global bound for both isotopes rapidly exceeding that set by ^{1}H alone if $g_d/g_p \neq 1$. For example, for both $g_d/g_p = 2$ and $g_d/g_p = 0$, we find that the upper bound on the possible value of $|g_e g_p|$ for NP bosons in the mass range 1–10 eV is strengthened by two orders of magnitude compared to that set using ^{1}H data alone and by a further factor of 5 when the Lamb shift measurements in muonic hydrogen and muonic deuterium are also taken into account.

The theoretical model of NP interaction considered in this work is outlined in Sec. II. Compared to previous work, we relax a number of assumptions: We do not make any assumptions about the new physics model being tested beyond those required to get to the Yukawa potential and we do not constrain the ratio of the coupling to the deuteron and the proton, or the sign of the NP shift. Bounds based on the whole of the current high-precision spectroscopic data are presented in Sec. III. Bounds based only on the isotope shift of the $1s_{1/2} - 2s_{1/2}$ interval [6] are also presented in this section. Prospects for further tightening the latter are discussed in Sec. IV. A recap of our main results is given in Sec. V. The main body of the paper is complemented by five Appendixes devoted to more technical details, including a discussion of the impact of a new physics interaction on the determination of the proton and deuteron charge radii from Lamb shift measurements in the muonic species.

II. NEW PHYSICS SCENARIOS

Most extensions of the standard model, which aim to explain the observation of excesses in the kinematic distributions of collision events or decays, require the introduction of propagating degrees of freedom that manifest as particles. To test the existence of such degrees of freedom and their interactions with standard model particles, it has become popular to parametrize a deformation of the standard model Lagrangian in terms of so-called simplified models [25].

Assuming a new force to be mediated through a spin-0 particle X_0 that couples to leptons and quarks with couplings g_{l_i} and g_{q_i}, respectively, we can expand the standard model Lagrangian $\mathcal{L}_{\mathrm{SM}}$ by

$$\mathcal{L} = \mathcal{L}_{\mathrm{SM}} + \sum_i (g_{l_i} \bar{l}_i l_i + g_{q_i} \bar{q}_i q_i) X_0. \tag{1}$$

Here i denotes the three flavor generations, and l_i and q_i refer to the mass basis of the SM fermions.[1]

With the Lagrangian of Eq. (1), the interaction mediated by the NP boson X_0 between an atomic nucleus and an electron or a muon contributes an additional Yukawa potential $V_{\mathrm{NP}}(r)$ to the Hamiltonian. In natural units,

$$V_{\mathrm{NP}}(r) = -\frac{g_l g_N}{4\pi} \frac{1}{r} e^{-m_{X_0} r}, \tag{2}$$

where r is the distance between the electron or muon and the nucleus and m_{X_0} is the particle's mass. Higher integer-spin

---

[1]An excellent review of such simplified models is provided in Ref. [9]. We also note that the interactions of Eq. (1) could be straightforwardly extended to (axial) vector or pseudoscalar particles and to flavor off-diagonal interactions, e.g., $g_{q_{ij}} \bar{q}_i q_j X_0$ with $i \neq j$.

mediators, e.g., vector particles, would also give rise to a Yukawa potential of this form. In general, for a massive force mediator of integer spin s,

$$V_{\mathrm{NP}}(r) = (-1)^{s+1} \frac{g_l g_N}{4\pi} \frac{1}{r} e^{-m_{X_0} r}. \tag{3}$$

However, assuming Lorentz invariance and the unitarity of the transition matrix element leads to an attractive (repulsive) force if $g_l g_N > 0$ ($g_l g_N < 0$) in the case of an even-spin mediator and to an attractive (repulsive) force if $g_l g_N < 0$ ($g_l g_N > 0$) in the case of an odd-spin mediator. To remain general, we allow positive and negative values for the product $g_l g_N$. We denote the coupling constant g_l by g_e for the case of an electron and g_μ for the case of a muon and the coupling constant g_N by g_p for the case of a proton and g_d for the case of a deuteron.

Such a new physics interaction would shift the energy of an (n, l) state of hydrogen or deuterium by a quantity $\delta E_{nl}^{\mathrm{NP}}$. The interaction is expected to be very weak. This energy shift does not need to be calculated beyond the first order in $V_{\mathrm{NP}}(r)$. The case of electronic hydrogen and electronic deuterium is straightforward: As noted, e.g., in our previous publication on this topic [7],

$$\delta E_{nl}^{\mathrm{NP}} = \int_0^\infty |R_{nl}(r)|^2 \frac{B \exp(-Cr)}{r} r^2 \mathrm{d}r, \tag{4}$$

where $R_{nl}(r)$ is the nonrelativistic radial wave function of the unperturbed state. The interaction potential is written in terms of the constants B and C rather than $g_l g_N$ and m_{X_0} to facilitate conversion from natural units to atomic units. To five significant figures,

$$B(E_\mathrm{h} a_0) = 10.905(-1)^{s+1} g_l g_N \tag{5}$$

and

$$C(a_0^{-1}) = 2.6817 \times 10^{-4} m_{X_0} \; (\mathrm{eV}). \tag{6}$$

As defined by the above equations, the coupling constant $g_l g_N$ is a pure number.

Relativistic wave functions must be used for muonic hydrogen and muonic deuterium. This case is addressed in Appendix A.

III. CURRENT BOUNDS ON THE STRENGTH OF AN NP INTERACTION

A. Methods

We only consider spectroscopic data in the present work, in view of the difficulty of deriving unambiguous results from the existing high-precision scattering data [26].

For electronic hydrogen (eH) and electronic deuterium (eD), the relevant spectroscopic data consist of a set of transition frequencies measured to a high degree of precision, i.e., $\nu_{b_1 a_1}^{\mathrm{expt}}$, $\nu_{b_2 a_2}^{\mathrm{expt}}$, $\nu_{b_3 a_3}^{\mathrm{expt}}$, etc. As in [7], we obtain bounds on the possible strength of a hypothetical NP interaction by comparing these measured frequencies to the prediction of the theoretical model outlined in Sec. II. Specifically, we compare each measured transition frequency $\nu_{b_i a_i}^{\mathrm{expt}}$ to its theoretical counterpart $\nu_{b_i a_i}^{\mathrm{th}}$, the latter being given by its standard model

value corrected for the NP shift defined by Eq. (4):

$$\nu_{b_i a_i}^{\text{th}} = \nu_{b_i a_i}^{\text{SM}} + \nu_{b_i a_i}^{\text{NP}}, \quad i = 1, 2, 3, \dots . \tag{7}$$

For a transition between a state a of principal quantum number n_a and orbital angular momentum quantum number l_a and a state b of principal quantum number n_b and orbital angular momentum quantum number l_b,

$$\nu_{ba}^{\text{NP}} = \left(\delta E_{n_b l_b}^{\text{NP}} - \delta E_{n_a l_a}^{\text{NP}}\right)/h, \tag{8}$$

where h is Planck's constant. Each SM transition frequency $\nu_{b_i a_i}^{\text{SM}}$ is the sum of a gross structure contribution $\nu_{b_i a_i}^{\text{g}}$ and various relativistic, QED, and hyperfine corrections [27–29]. These various contributions depend on the Rydberg frequency $\mathcal{R}$ and some also depend on the charge radius of the proton r_p and the charge radius of the deuteron r_d. As in [7], we group them into a gross structure term depending sensitively on $\mathcal{R}$, terms depending sensitively on r_p or r_d, and a term accounting for all the other contributions to the SM transition frequency. Specifically, we write

$$\nu_{b_i a_i}^{\text{SM}} = \mathcal{R}\, \tilde{\nu}_{b_i a_i}^{\text{g}} + r_p^2\, \tilde{\nu}_{b_i a_i}^{\text{ps}} + r_d^2\, \tilde{\nu}_{b_i a_i}^{\text{ds}} + \nu_{b_i a_i}^{\text{oc}}, \tag{9}$$

where the factors $\tilde{\nu}_{b_i a_i}^{\text{g}}$, $\tilde{\nu}_{b_i a_i}^{\text{ps}}$, and $\tilde{\nu}_{b_i a_i}^{\text{ds}}$ and the term $\nu_{b_i a_i}^{\text{oc}}$ do not strongly depend on the precise values of $\mathcal{R}$, r_p, and r_d, if they depend on them at all. In particular,

$$\tilde{\nu}_{b_i a_i}^{\text{g}} = \nu_{b_i a_i}^{\text{g}}/\mathcal{R} = \left(\frac{1}{n_{a_i}^2} - \frac{1}{n_{b_i}^2}\right)\frac{m_{\text{r}}}{m_e}, \tag{10}$$

where m_{r} is the reduced mass of the atom and m_e is the mass of the electron. The proton size and deuteron size terms $r_p^2\, \tilde{\nu}_{b_i a_i}^{\text{ps}}$ and $r_d^2\, \tilde{\nu}_{b_i a_i}^{\text{ds}}$, respectively, group the QED contributions which are roughly proportional to r_p^2 and r_d^2, respectively, and the term $\nu_{b_i a_i}^{\text{oc}}$ encapsulates all the other corrections to the gross structure contribution.

The data for muonic hydrogen (μH) and muonic deuterium (μD) are currently limited to high-precision measurements of the Lamb shift of the $n = 2$ states. In principle, these data could be integrated in the calculation of NP bounds exactly as described in the preceding paragraph. However, it is more convenient to use a slightly different (albeit equivalent) formulation, which is more closely related to the QED theory of these species. Specifically, we write the theoretical Lamb shift of muonic hydrogen $\Delta E_{\mu\text{H}}^{\text{th}}$ as a sum of a term proportional to the square of the proton charge radius, a term which does not depend sensitively on this radius, and a new physics contribution, and similarly for the theoretical Lamb shift of muonic deuterium ($\Delta E_{\mu\text{D}}^{\text{th}}$):

$$\Delta E_{\mu\text{H}}^{\text{th}} = \Delta E_{\mu\text{H}}^{\text{main}} + r_p^2\, \tilde{\Delta} E_{\mu\text{H}}^{\text{ns}} + \Delta E_{\mu\text{H}}^{\text{NP}}, \tag{11}$$

$$\Delta E_{\mu\text{D}}^{\text{th}} = \Delta E_{\mu\text{D}}^{\text{main}} + r_d^2\, \tilde{\Delta} E_{\mu\text{D}}^{\text{ns}} + \Delta E_{\mu\text{D}}^{\text{NP}}. \tag{12}$$

The QED theory of these species [30,31] yields $\Delta E_{\mu\text{H}}^{\text{main}} = 206.0668(25)$ meV, $\tilde{\Delta} E_{\mu\text{H}}^{\text{ns}} = -5.2275(10)$ meV/fm^2, $\Delta E_{\mu\text{D}}^{\text{main}} = 230.5283(200)$ meV, and $\tilde{\Delta} E_{\mu\text{D}}^{\text{ns}} = -6.108\,01(28)$ meV/fm^2. We calculate the new physics correction terms $\Delta E_{\mu\text{H}}^{\text{NP}}$ and $\Delta E_{\mu\text{D}}^{\text{NP}}$ as described in Appendix A (the calculation is based on the Dirac equation and takes into account the nuclear charge distribution and vacuum polarization). Equating $\Delta E_{\mu\text{H}}^{\text{th}}$ and $\Delta E_{\mu\text{D}}^{\text{th}}$ to the experimental Lamb shifts [30,32] yields NP-corrected values for r_p and r_d.

We codetermine $\mathcal{R}$, r_p, and r_d and confidence levels of the NP coupling constants by a global correlated χ^2 fit of our theoretical model to experiment [33]. Specifically, given values of g_p, g_d, g_e, g_μ, and m_{X_0} characterizing an NP interaction, we adjust $\mathcal{R}$, r_p, and r_d so as to minimize the difference between the theoretical transition frequency $\nu_{b_i a_i}^{\text{th}}$ and the corresponding experimental transition frequency $\nu_{b_i a_i}^{\text{expt}}$ for each of the transitions considered. In calculations including the muonic species, we also minimize the difference between the charge radii derived from measurements in the electronic species from those derived from measurements in the muonic species. The resulting value of χ^2 characterizes how close the theory fits the data for given values of g_p, g_d, g_e, g_μ, and m_{x_0}. Having this value, we calculate the upper tail cumulative distribution function $Q(\chi^2|\nu) = 1 - P(\chi^2|\nu)$ for the relevant number of degrees of freedom ν. Here $Q(\chi^2|\nu)$ is the probability that the difference between theory and experiment arises only from random experimental and theoretical errors. A small value of this probability indicates a low likelihood that the data are compatible with a new physics interaction of the type considered in this work. The calculation is essentially the same as that underpinning the determination of $\mathcal{R}$, r_p, and r_d by CODATA [27,29], albeit here limited to the spectroscopic data and generalized to the encompass the possibility of an NP interaction. Further details can be found in [7] and in Appendix B.

B. Bounds based on spectroscopic measurements in eH and eD

Fitting solely against the hydrogen data yields the results shown in Fig. 1(a) for an attractive NP interaction and in Fig. 1(b) for a repulsive NP interaction. The shades of green indicate the extent to which the data are compatible with the presence of the interaction, as per the color axis. The white regions correspond to areas where an NP interaction is excluded at the 95% confidence level (i.e., areas where the probability that the data are compatible with an NP interaction is less than 0.05). We take the boundaries delineating the white and green regions as defining upper bounds on the values of $g_e g_p$ consistent with the current experimental evidence, as determined in this particular analysis. These bounds are highlighted by black curves for better visibility. For comparison, the gray curves represent the corresponding bounds found in [7] for the largest data set considered in this previous work, "data set A." This data set did not include recent measurements, which are taken into account in the present work (namely, measurements of the $2p_{1/2} - 2s_{1/2}$, $1s_{1/2} - 3s_{1/2}$, and $2s_{1/2} - 8d_{5/2}$ intervals [34–36]). Compared to [7], the bounds found for the more extensive data set considered here are tighter for an attractive interaction and slightly less tight for a repulsive interaction, except in the low-mass region, where they are similar. However, it should be noted that the confidence levels remain low at all values of $g_e g_p$, reflecting the well-known inconsistencies between some of the data.

Fitting solely against the deuterium data yields the results shown in Figs. 1(c) and 1(d). These data exhibit a higher consistency level than hydrogen, which translates into higher confidence levels at low values of $|g_e g_d|$. For mediator masses
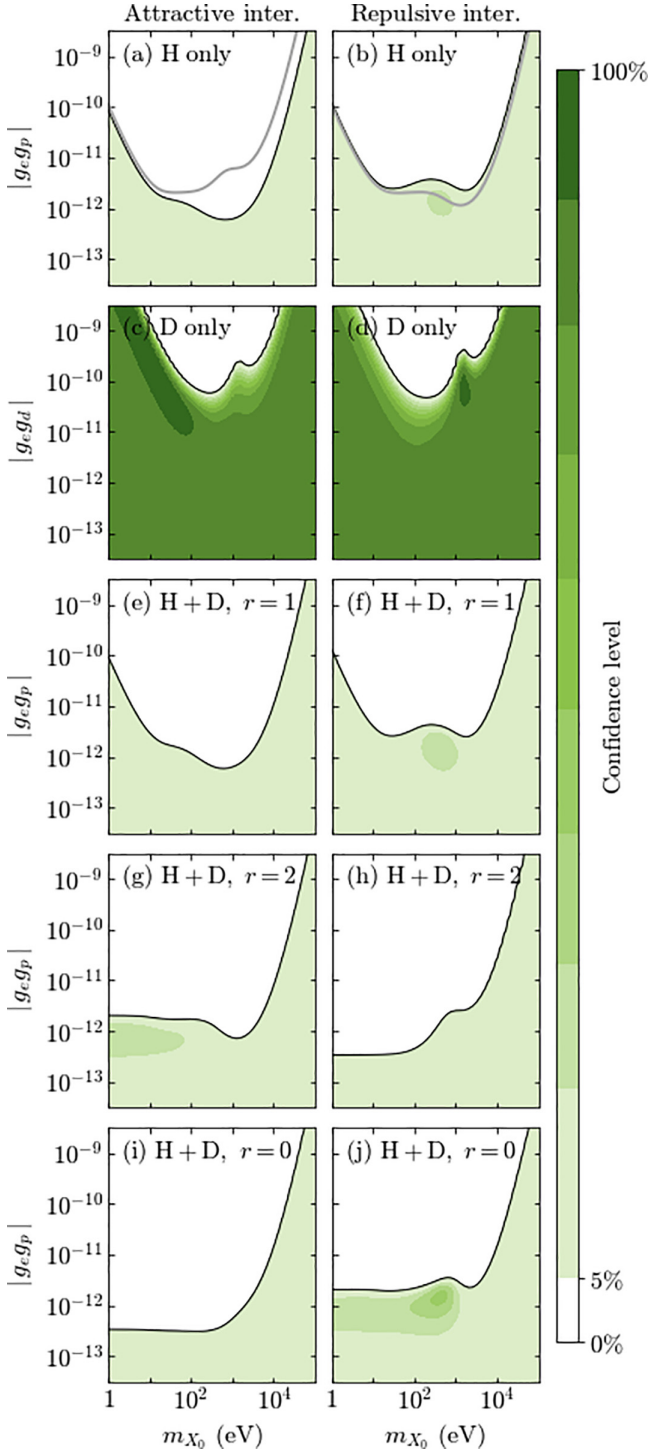
FIG. 1. Confidence level that an NP interaction is compatible with the world spectroscopic data for electronic ^{1}H and/or electronic deuterium. (a) and (b) Results solely based on the ^{1}H data. (c) and (d) Results solely based on the deuterium data. (e)–(j) Results obtained by combining the ^{1}H and deuterium data, assuming that the ratio $r = g_d/g_p$ is either (e) and (f) 1, (g) and (h) 2, or (i) and (j) 0. The left column refers to an attractive NP interaction and the right column to a repulsive NP interaction. The possibility of an NP interaction with parameters falling in a white region is excluded at the 95% confidence level. The black curves show the corresponding upper bounds on the value of $g_e g_p$ or $g_e g_d$. The gray curves show the upper bounds on the value of $g_e g_p$ found in Ref. [7].
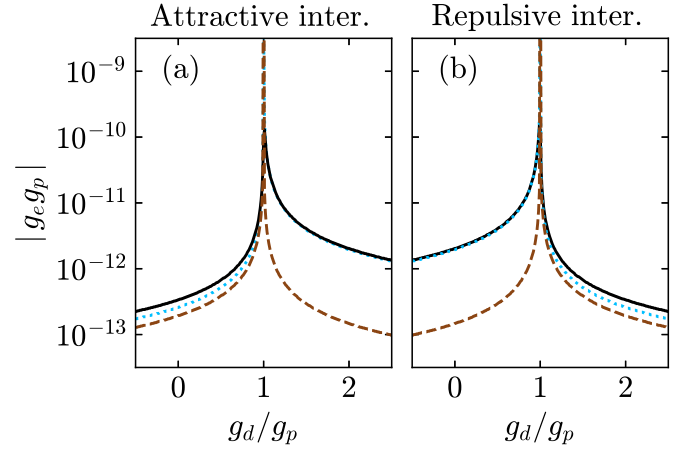

FIG. 2. Value of $|g_e g_p|$ above which an NP interaction is excluded at the 95% confidence level, assuming that $m_{X_0} = 1$ eV, vs the ratio g_d/g_p. (a) Attractive NP interaction. (b) Repulsive NP interaction. The black solid curves show results based on the world spectroscopic data, as in Figs. 1(e)–1(j). The blue dotted curves show the same results but now excluding those for the high Rydberg states. The brown dashed curves show isotope shift results as in Fig. 5.

below 100 eV, the bounds on $|g_e g_d|$ set by the deuterium data are considerably less stringent than those on $|g_e g_p|$ set by the hydrogen data. The latter is strengthened in this region by measurements on high Rydberg states, which are not available for deuterium [2,7].

Combining the hydrogen data with the deuterium data yields the results shown in Figs. 1(e)–1(j), for three different ratios of the respective coupling constants. We denote this ratio by r:

$$r = g_d/g_p. \tag{13}$$

The confidence levels for $g_d = g_p$ ($r = 1$) hardly differ from those solely based on the hydrogen data, which should be expected since the hydrogen data place a stronger constraint on the product $g_e g_p$ than the deuterium data do on the product $g_e g_d$.

However, taking $g_d \neq g_p$ creates a mismatch in the NP shift of the transition frequencies between the two isotopes, which generally diminishes the data's compatibility with the presence of an NP interaction. As shown by these figures, the mismatch created by assuming that $g_d = 2g_p$ ($r = 2$) or that $g_d = 0$ ($r = 0$) rather than $g_d = g_p$ does not significantly impact the bound on $g_e g_p$ for masses above 1 keV. For lower masses, however, it shifts this bound towards substantially smaller values of $|g_e g_p|$. As illustrated by Fig. 2, this bound on $g_e g_p$ tightens very rapidly in the low-mass region as soon as r starts departing from 1. Figure 2 also shows that it is only for $r = 1$ that the high Rydberg state datum is important for constraining $g_e g_p$ (compare the blue dotted curves to the black solid curves): For any other values of r, the bounds on $g_e g_p$ depend little on whether the measurements on Rydberg states are taken into account.

One may also note that the results of Figs. 1(a)–1(j) tend to favor nonzero values of $g_e g_p$ in certain ranges of mediator masses; however, the difference in confidence level with

TABLE I. Value of $|g_e g_p|$ above which an NP interaction is excluded at the 95% confidence level, for different values of m_{X_0} (the mass of the NP carrier) and different values of the ratio g_μ/g_e, as calculated in the isotope shift approach for $g_d/g_p = 2$. The numbers within square brackets indicate multiplication by powers of 10.

m_{X_0}	$g_\mu = 0$	$g_\mu = g_e$	$g_\mu = 10g_e$	$g_\mu = 100g_e$
		Attractive NP interaction		
$\leqslant 100$ eV	1.5[−13]	1.5[−13]	1.5[−13]	1.5[−13]
1 keV	1.7[−13]	1.7[−13]	1.7[−13]	1.7[−13]
10 keV	6.8[−13]	6.8[−13]	6.8[−13]	6.8[−13]
100 keV	2.6[−11]	2.6[−11]	2.6[−11]	2.7[−11]
1 MeV	2.3[−9]	2.6[−9]	1.2[−7]	3.3[−10]
10 MeV	2.3[−7]	8.8[−7]	4.6[−8]	4.1[−9]
		Repulsive NP interaction		
$\leqslant 100$ eV	1.9[−13]	1.9[−13]	1.9[−13]	1.9[−13]
1 keV	2.2[−13]	2.2[−13]	2.2[−13]	2.2[−13]
10 keV	8.9[−13]	8.9[−13]	8.9[−13]	8.9[−13]
100 keV	3.4[−11]	3.4[−11]	3.4[−11]	3.5[−11]
1 MeV	3.0[−9]	3.4[−9]	8.8[−8]	2.5[−10]
10 MeV	3.0[−7]	1.2[−6]	3.5[−8]	3.1[−9]

$g_e g_p = g_e g_d = 0$ is too small to point towards the possible existence of an NP interaction.

C. Bounds based on spectroscopic measurements in eH, eD, μH, and μD

Adding the muonic hydrogen and muonic deuterium measurements to the data used in the preceding section makes it necessary to ascertain the role of an NP interaction on the intervals measured in these species. The issue is discussed in Appendix A. We find that an NP interaction with a carrier mass below 10 keV is unlikely to shift these intervals significantly, unless this interaction would couple to a muon much more strongly than to an electron ($|g_\mu| \gg |g_e|$). However, the situation is less clear for higher carrier masses, even for $g_\mu \approx g_e$.

Accordingly, we allow for the possibility that an NP interaction plays a role in the measurements of the muonic species. As described in Sec. III A, we do this by correcting r_p and r_d for a hypothetical NP shift and use these corrected values when fitting theory to experiment. Bounds can also be obtained by following the method outlined in Appendix C, which is more limited in scope and produces almost identical results where comparison is possible. Either way, the confidence levels derived from these calculations depend on the relative values of the coupling constants g_μ and g_e. For simplicity, we assumed that $g_\mu = g_e$ for producing the figures presented in this section. Results calculated for other relative values of g_μ can be found in Table I and are discussed below.

As is well known, however, the nuclear radii derived from the measurements in muonic hydrogen and muonic deuterium are in severe tension with much of the high-precision data currently available for electronic hydrogen and electronic deuterium [37]. These inconsistencies hamper calculations of bounds combining muonic and electronic species to the extent that our theoretical model cannot be made to match the whole
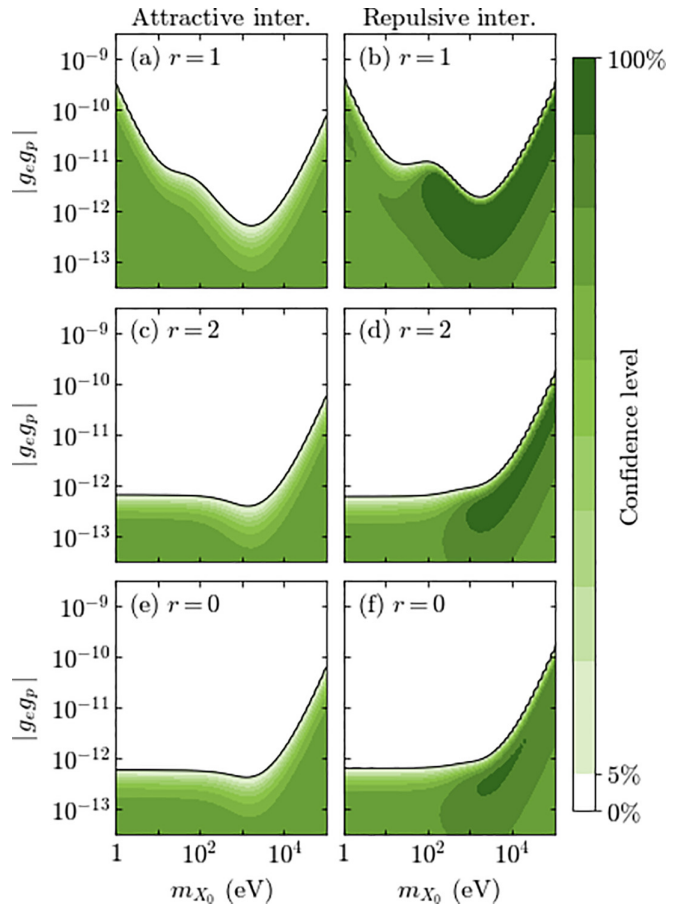

FIG. 3. Confidence level that an NP interaction is compatible with the world spectroscopic data for electronic ^{1}H, electronic deuterium, muonic hydrogen, and muonic deuterium, assuming that the ratio $r = g_d/g_p$ is either (a) and (b) 1, (c) and (d) 2, or (e) and (f) 0 and that $g_\mu = g_e$. The left column refers to an attractive NP interaction and the right column to a repulsive NP interaction. All experimental uncertainties have been increased by 60%. As in Fig. 1, the possibility of an NP interaction with parameters falling in a white region is excluded at the 95% confidence level and the black curves indicate the corresponding upper bounds on the value of $g_e g_p$.

set of data for any value of $g_e g_p$ when $g_d \neq g_p$. The model cannot be made to match the data for an attractive NP interaction, whereas a match with a relatively weak confidence level (up to 38%) is found at nonzero values of $g_e g_p$ for a repulsive interaction (see Appendix D). The better match found in the latter case illustrates the fact, already known [7,8,36], that including a weak NP interaction in the theoretical model may improve its overall agreement with the world data. However, the relevance of this result is unclear given the residual inconsistencies within this data.

CODATA alleviated the difficulty of fitting the data to the standard model theory by increasing all the experimental uncertainties by 60% [29]. Doing so yields the bounds and distributions of confidence level presented in Fig. 3, for masses up to 100 keV, and in Fig. 4 (the black curves), for masses above 100 keV. Comparing with Fig. 1 shows that taking the muonic data into account tightens the bounds on NP further, by a considerable extent above 100 keV, despite the
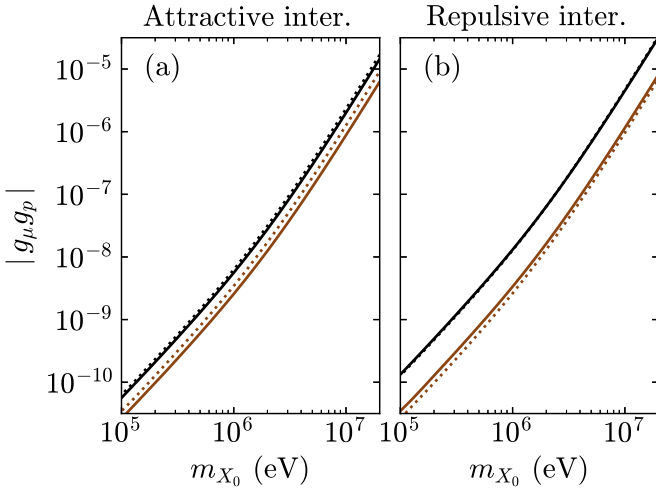
FIG. 4. Value of $|g_e g_p|$ above which an NP interaction is excluded at the 95% confidence level, assuming that the ratio g_d/g_p is either 2 (solid curves) or 0 (dotted curves) and that $g_\mu = g_e$, for a mediator mass above 1×10^5 eV. (a) Attractive NP interaction. (b) Repulsive NP interaction. The black curves show results based on the world spectroscopic data as in Fig. 3. The brown curves show results based only on the isotope shift measurements as in Fig. 5.
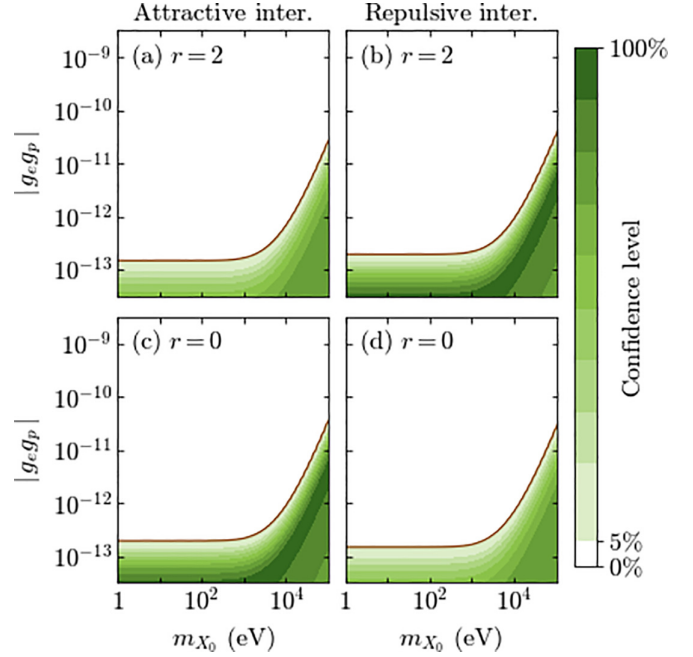

FIG. 5. Confidence level that an NP interaction is compatible with the $1s_{1/2} - 2s_{1/2}$ transition frequency measured in electronic hydrogen and electronic deuterium and with the nuclear charge radii derived from measurements in muonic hydrogen and muonic deuterium, assuming that the ratio $r = g_d/g_p$ is either (a) and (b) 2 or (c) and (d) 0 and that $g_\mu = g_e$. The experimental uncertainties are not changed here. The left column refers to an attractive NP interaction and the right column to a repulsive NP interaction. As in Fig. 1, the possibility of an NP interaction with parameters falling in a white region is excluded at the 95% confidence level. The brown curves indicate the corresponding upper bounds on the value of $g_e g_p$.

larger experimental uncertainties assumed in the calculation. (Results for an error magnification of 20% rather than 60% can be found in Appendix D, for comparison.)

The difficulty of fitting the theoretical model to experiment can also be turned around without magnifying the experimental uncertainties by using only selected subsets of the available data. For $g_d \neq g_p$, the tightest bounds are obtained by combining the muonic values of the nuclear radii with the isotope shift of the $1s_{1/2} - 2s_{1/2}$ transition in the electronic species, owing to the particularly small experimental errors on these quantities.[2] The results for $r = 0$ or 2 are presented in Fig. 4 (the brown curves) and in Fig. 5. They are also tabulated in Table I for $r = 2$ (the column headed $g_\mu = g_e$). We do not present results for $r = 1$, as this approach is unsuitable for this case (see Appendix C). Compared to the results of Figs. 3(c)–3(f), the bounds obtained in this approach are significantly tighter. As in the case of the results based only on the electronic species, they vary with the ratio r and strengthen rapidly when this ratio starts departing from 1 (see the brown dashed curves in Fig. 2). We also note the sensitivity of these results to the details of small QED corrections. The theory of the Lamb shift in muonic deuterium has been further extended over the past few years [31,32,39]. As shown in Appendix D, these new theoretical developments have significantly impacted on the conclusions one could draw from the isotope shift data in respect to the bounds on a hypothetical NP interaction.

How these bounds vary with the ratio g_μ/g_e is illustrated by Table I. They do not significantly depend on the value of this ratio for mediator masses up to about 100 keV. At higher masses, however, they tend to move to higher values of $|g_e g_p|$ as g_μ/g_e increases, pass through a maximum, and become tighter again for still higher values of this ratio. The maximum is reached at around or above 10 MeV for $g_\mu \approx g_e$ and at around 1 MeV for higher values of g_μ/g_e. Except in that mass region, taking $g_\mu = g_e$ in the calculation of these bounds is therefore a conservative assumption.

IV. REACH OF THE ISOTOPE SHIFT APPROACH

The bounds on $g_e g_p$ discussed in the preceding section are based on the current experimental evidence. We now consider the prospects for further tightening these bounds. Specifically, we look at how future isotope shift measurements could be used to this effect. We address this issue by using a method similar to that outlined in Appendix C for the specific case of the $1s_{1/2} - 2s_{1/2}$ interval, here generalized to other transitions. In effect, we also generalize the isotope shift calculations reported in Ref. [6].

_____

[2]This approach was followed in Ref. [6], with similar results, although with one important difference: The authors of Ref. [6] neglected the difference between the theoretical and experimental shifts [38] whereas we do not. As a result, the bound reported in Ref. [6] is actually a measure of the sensitivity of the isotope shift approach rather than a bound in the sense of the present work.

A. Bounds based on a single isotope shift

1. Method

The case of a single transition is particularly simple. Let us assume that a transition from a state a to a state b has been measured both in hydrogen and in deuterium, the result being the transition frequencies $\nu_{ba,\mathrm{eH}}^{\mathrm{expt}}$ and $\nu_{ba,\mathrm{eD}}^{\mathrm{expt}}$. We equate these two experimental transition frequencies to the corresponding theoretical transition frequencies, the latter including a possible NP shift:

$$\nu_{ba,\mathrm{eH}}^{\mathrm{expt}} = \mathcal{R}\tilde{\nu}_{ba,\mathrm{eH}}^{\mathrm{g}} + r_p^2\,\tilde{\nu}_{ba,\mathrm{eH}}^{\mathrm{ns}} + \nu_{ba,\mathrm{eH}}^{\mathrm{oc}} + \nu_{ba,\mathrm{eH}}^{\mathrm{NP}}, \tag{14}$$

$$\nu_{ba,\mathrm{eD}}^{\mathrm{expt}} = \mathcal{R}\tilde{\nu}_{ba,\mathrm{eD}}^{\mathrm{g}} + r_d^2\,\tilde{\nu}_{ba,\mathrm{eD}}^{\mathrm{ns}} + \nu_{ba,\mathrm{eD}}^{\mathrm{oc}} + \nu_{ba,\mathrm{eD}}^{\mathrm{NP}}. \tag{15}$$

As above, $\mathcal{R}$ is the Rydberg frequency, $\nu_{ba,\mathrm{eH}}^{\mathrm{NP}}$ and $\nu_{ba,\mathrm{eD}}^{\mathrm{NP}}$ are NP shifts, $r_p^2\tilde{\nu}_{ba,\mathrm{eH}}^{\mathrm{ns}}$ and $r_d^2\tilde{\nu}_{ba,\mathrm{eD}}^{\mathrm{ns}}$ are QED corrections proportional to the square of the respective nuclear radius, and $\nu_{ba,\mathrm{eH}}^{\mathrm{oc}}$ and $\nu_{ba,\mathrm{eD}}^{\mathrm{oc}}$ are the sums of all the other SM corrections to the gross structure terms $\mathcal{R}\tilde{\nu}_{ba,\mathrm{eH}}^{\mathrm{g}}$ and $\mathcal{R}\tilde{\nu}_{ba,\mathrm{eD}}^{\mathrm{g}}$. We will denote the corresponding isotope shifts by $\Delta\nu_{ba}^{\mathrm{expt}}$, $\Delta\nu_{ba}^{\mathrm{g}}$, $\Delta\nu_{ba}^{\mathrm{ns}}$, $\Delta\nu_{ba}^{\mathrm{oc}}$, and $\Delta\nu_{ba}^{\mathrm{NP}}$:

$$\Delta\nu_{ba}^{\mathrm{expt}} = \nu_{ba,\mathrm{eD}}^{\mathrm{expt}} - \nu_{ba,\mathrm{eH}}^{\mathrm{expt}}, \tag{16}$$

$$\Delta\nu_{ba}^{\mathrm{g}} = \mathcal{R}\tilde{\nu}_{ba,\mathrm{eD}}^{\mathrm{g}} - \mathcal{R}\tilde{\nu}_{ba,\mathrm{eH}}^{\mathrm{g}}, \tag{17}$$

$$\Delta\nu_{ba}^{\mathrm{ns}} = r_d^2\,\tilde{\nu}_{ba,\mathrm{eD}}^{\mathrm{ns}} - r_p^2\,\tilde{\nu}_{ba,\mathrm{eH}}^{\mathrm{ns}}, \tag{18}$$

$$\Delta\nu_{ba}^{\mathrm{oc}} = \nu_{ba,\mathrm{eD}}^{\mathrm{oc}} - \nu_{ba,\mathrm{eH}}^{\mathrm{oc}}, \tag{19}$$

$$\Delta\nu_{ba}^{\mathrm{NP}} = \nu_{ba,\mathrm{eD}}^{\mathrm{NP}} - \nu_{ba,\mathrm{eH}}^{\mathrm{NP}}. \tag{20}$$

As given by Eq. (10),

$$\Delta\nu_{ba}^{\mathrm{g}} = \mathcal{R}\left[\frac{m_{\mathrm{r}}^{\mathrm{eD}}}{m_e} - \frac{m_{\mathrm{r}}^{\mathrm{eD}}}{m_e}\right]\left(\frac{1}{n_a^2} - \frac{1}{n_b^2}\right), \tag{21}$$

where $m_{\mathrm{r}}^{\mathrm{eH}}$ ($m_{\mathrm{r}}^{\mathrm{eD}}$) is the reduced masses of electronic hydrogen (deuterium) and m_e is the mass of the electron. To conform with previous work on the isotope shift [40,41], and contrary to Sec. III A, we only include the main nuclear size correction in $\Delta\nu_{ba}^{\mathrm{ns}}$. Thus

$$\Delta\nu_{ba}^{\mathrm{ns}} = -\frac{2\alpha^4 m_e c^2}{3h}\left[\left(\frac{m_{\mathrm{r}}^{\mathrm{eD}}}{m_e}\right)^3\frac{r_d^2}{\lambdabar_{\mathrm{C}}^2} - \left(\frac{m_{\mathrm{r}}^{\mathrm{eH}}}{m_e}\right)^3\frac{r_p^2}{\lambdabar_{\mathrm{C}}^2}\right]$$
$$\times\left(\frac{\delta_{l_a,0}}{n_a^3} - \frac{\delta_{l_b,0}}{n_b^3}\right) \tag{22}$$

and $\Delta\nu_{ba}^{\mathrm{oc}}$ includes all the other corrections to the gross structure term.

We now use the fact that $\nu_{ba,\mathrm{eH}}^{\mathrm{NP}}$ is proportional to $g_e g_p$ and $\nu_{ba,\mathrm{eD}}^{\mathrm{NP}}$ to $g_e g_d$. Since $g_e g_d = r g_e g_p$, where r is defined by Eq. (13), $\nu_{ba,\mathrm{eH}}^{\mathrm{NP}}$, $\nu_{ba,\mathrm{eD}}^{\mathrm{NP}}$, and $\Delta\nu_{ba}^{\mathrm{NP}}$ can be written in terms of $g_e g_p$-independent shifts $\tilde{\nu}_{ba,\mathrm{eH}}^{\mathrm{NP}}$, $\tilde{\nu}_{ba,\mathrm{eD}}^{\mathrm{NP}}$, and $\Delta\tilde{\nu}_{ba}^{\mathrm{NP}}$, namely,

$$\nu_{ba,\mathrm{eH}}^{\mathrm{NP}} = g_e g_p\,\tilde{\nu}_{ba,\mathrm{eH}}^{\mathrm{NP}}, \tag{23}$$

$$\nu_{ba,\mathrm{eD}}^{\mathrm{NP}} = r\,g_e g_p\,\tilde{\nu}_{ba,\mathrm{eD}}^{\mathrm{NP}}, \tag{24}$$

$$\Delta\nu_{ba}^{\mathrm{NP}} = g_e g_p\,\tilde{\nu}_{ba}^{\mathrm{NP}}, \tag{25}$$

with

$$\Delta\tilde{\nu}_{ba}^{\mathrm{NP}} = r\tilde{\nu}_{ba,\mathrm{eD}}^{\mathrm{NP}} - \tilde{\nu}_{ba,\mathrm{eH}}^{\mathrm{NP}}. \tag{26}$$

Subtracting Eq. (14) from Eq. (15) and rearranging yields

$$g_e g_p = \frac{\Delta\nu_{ba}^{\mathrm{expt}} - \Delta\nu_{ba}^{\mathrm{SM}}}{\Delta\tilde{\nu}_{ba}^{\mathrm{NP}}}, \tag{27}$$

where

$$\Delta\nu_{ba}^{\mathrm{SM}} = \Delta\nu_{ba}^{\mathrm{g}} + \Delta\nu_{ba}^{\mathrm{ns}} + \Delta\nu_{ba}^{\mathrm{oc}}. \tag{28}$$

Equation (27) gives the strength of a hypothetical NP interaction which would explain a discrepancy between a measured transition frequency and the value predicted by the standard model. However, because of the measurements' finite precision and the theoretical uncertainties in the QED corrections, this equation defines this strength only approximately. We denote the errors on $\Delta\nu_{ba}^{\mathrm{expt}}$ and $\Delta\nu_{ba}^{\mathrm{SM}}$ by $\sigma_{ba}^{\mathrm{expt}}$ and $\sigma_{ba}^{\mathrm{SM}}$ and the total error on the numerator of Eq. (27) by σ_{ba}:

$$\sigma_{ba} = \sqrt{\left(\sigma_{ba}^{\mathrm{expt}}\right)^2 + \left(\sigma_{ba}^{\mathrm{SM}}\right)^2}. \tag{29}$$

The value of $g_e g_p$ predicted by Eq. (27) has a 95% confidence interval of $\pm\sigma(|g_e g_p|)$, where[3]

$$\sigma(|g_e g_p|) = 1.96\sigma_{ba}/\Delta\tilde{\nu}_{ba}^{\mathrm{NP}}. \tag{30}$$

It should be noted that $\sigma(|g_e g_p|)$ is not a bound on the strength of the NP interaction. Rather, $\sigma(|g_e g_p|)$ is half the difference between the most positive and most negative values of $g_e g_p$ consistent with this interaction. The value of $\sigma(|g_e g_p|)$ thus indicates the sensitivity of the method. Equations (29) and (30) show that this sensitivity is determined by the values of $\sigma_{ba}^{\mathrm{expt}}$, $\sigma_{ba}^{\mathrm{SM}}$, and $\Delta\tilde{\nu}_{ba}^{\mathrm{NP}}$ for the interval considered. Since $\sigma(|g_e g_p|)$ is inversely proportional to $\Delta\tilde{\nu}_{ba}^{\mathrm{NP}}$ and $\Delta\tilde{\nu}_{ba}^{\mathrm{NP}}$ is particularly small for $g_d \approx g_p$, the method is unsuited to the $r = 1$ case.

In regard to the measurements, we assume errors $\sigma_{ba,\mathrm{eD}}^{\mathrm{expt}}$ and $\sigma_{ba,\mathrm{eH}}^{\mathrm{expt}}$ on $\nu_{ba,\mathrm{eD}}^{\mathrm{expt}}$ and $\nu_{ba,\mathrm{eH}}^{\mathrm{expt}}$ taken individually and an error $\sigma_{ba}^{\mathrm{expt}}$ on the difference $\nu_{ba,\mathrm{eD}}^{\mathrm{expt}} - \nu_{ba,\mathrm{eH}}^{\mathrm{expt}}$. Assuming that $\sigma_{ba,\mathrm{eD}}^{\mathrm{expt}}$ and $\sigma_{ba,\mathrm{eH}}^{\mathrm{expt}}$ are uncorrelated,

$$\sigma_{ba}^{\mathrm{expt}} = \sqrt{\left(\sigma_{ba,\mathrm{eD}}^{\mathrm{expt}}\right)^2 + \left(\sigma_{ba,\mathrm{eH}}^{\mathrm{expt}}\right)^2}. \tag{31}$$

Regarding the standard model theory, we note that

$$\sigma_{ba}^{\mathrm{SM}} = \sqrt{\left(\sigma_{ba}^{\mathrm{g}}\right)^2 + \left(\sigma_{ba}^{\mathrm{ns}}\right)^2 + \left(\sigma_{ba}^{\mathrm{oc}}\right)^2}, \tag{32}$$

where σ_{bg}^{g}, $\sigma_{ba}^{\mathrm{ns}}$, and $\sigma_{ba}^{\mathrm{oc}}$ are the errors on the gross structure term $\Delta\nu_{ba}^{\mathrm{g}}$, on the nuclear size term $\Delta\nu_{ba}^{\mathrm{ns}}$, and on the other corrections term $\Delta\nu_{ba}^{\mathrm{oc}}$.

We first consider the error on the gross structure term. Using the CODATA 2018 values of the mass ratios m_e/m_p and m_e/m_d and the correlation in their uncertainties [29],

$$\frac{m_{\mathrm{r}}^{\mathrm{eD}}}{m_e} - \frac{m_{\mathrm{r}}^{\mathrm{eH}}}{m_e} = 2.719\,510\,698\,49(31) \times 10^{-4}. \tag{33}$$

---

[3]There is no need to consider the error on $\Delta\tilde{\nu}_{ba}^{\mathrm{NP}}$ here, which arises from the uncertainty on the reduced masses, the use of nonrelativistic wave functions, etc., as this error is dwarfed by σ_{ba}.

The relative error on this result, 1.1×10^{-10}, is two orders of magnitude larger than the relative error on the Rydberg frequency [29]. The error on the gross structure term is therefore dominated by the error on the difference of mass ratios. We find[4]

$$\sigma_{ba}^{\mathrm{g}} = 0.10 \text{ kHz} \times \left(\frac{1}{n_a^2} - \frac{1}{n_b^2} \right). \tag{34}$$

The error on the nuclear size term is dominated by the error on r_p^2 and particularly by the more significant error on r_d^2. The other quantities in Eq. (22) have a negligible error. We use the radii derived from the Lamb shift in muonic hydrogen and muonic deuterium, here recalculated to take into account a hypothetical NP interaction (we set $g_\mu = g_e$ when obtaining the numerical results presented in this section). We find that the errors on these radii do not significantly vary with $g_e g_p$ in the range of values of $g_e g_p$ relevant for this work. They can be taken to be equal to the values determined without allowance for an NP interaction [30,31], which gives

$$\sigma_{ba}^{\mathrm{ns}} = 5.3 \text{ kHz} \times \left(\frac{\delta_{l_a,0}}{n_a^3} - \frac{\delta_{l_b,0}}{n_b^3} \right). \tag{35}$$

The error on the other corrections term can be derived from previous work [40,41]. In particular, Pachucki *et al.* [41] obtained 0.42 kHz for the total error on the theoretical $1s_{1/2} - 2s_{1/2}$ transition frequency, excluding errors that we include in $\sigma_{ba}^{\mathrm{ns}}$ or σ_{ba}^{g} in the present work (i.e., the error on the leading nuclear size contribution and the error on the Dirac contribution to the isotope shift). Accordingly, we take $\sigma_{ba}^{\mathrm{oc}}$ to be 0.42 kHz for the $1s_{1/2} - 2s_{1/2}$ interval. The main contribution to this error comes from the dominant QED corrections, which scale with the principal quantum number n like $1/n^3$. Some subdominant corrections have a more complicated scaling with n; however, they are negligible in the present context. Hence, for transitions between two s states, we set

$$\sigma_{ba}^{\mathrm{oc}} = 0.48 \text{ kHz} \times \left(\frac{1}{n_a^3} - \frac{1}{n_b^3} \right), \tag{36}$$

which ensures that $\sigma_{ba}^{\mathrm{oc}} = 0.42$ kHz for $n_a = 1$ and $n_b = 2$. For transitions between s states, both σ_{ba}^{g} and $\sigma_{ba}^{\mathrm{oc}}$ are thus typically one order of magnitude smaller than $\sigma_{ba}^{\mathrm{ns}}$. Consequently, the method's sensitivity for such transitions is primarily limited by the experimental error and the uncertainty on the nuclear charge radii.

The error on the Lamb shift is considerably smaller for p or d states than for s states of the same principal quantum number. Setting $\sigma_{ba}^{\mathrm{oc}}$ equal to 0 for intervals not involving s states is thus appropriate, which results in a smaller value of σ_{ba} for the same experimental error. However, the gain in sensitivity arising from this smaller overall error may be partly or entirely negated by a smaller value of $\Delta \tilde{\nu}_{ba}^{\mathrm{NP}}$ (transitions not involving s states are necessarily transitions between two excited states, and the NP shift of such transitions is always smaller than the NP shift of a transition between the ground state and an excited state).

---

[4]Using the value of the proton mass obtained by Heiße *et al.* [42] rather than the CODATA 2018 value would reduce this error to 0.085 kHz $\times (1/n_a^2 - 1/n_b^2)$.

TABLE II. Sensitivity parameter $\sigma(|g_e g_p|)$ for $m_{X_0} \lesssim 1$ eV, $g_d/g_p = 2$, and $g_\mu/g_e = 1$, as calculated from the isotope shift of each of the transitions indicated in the first column. The second column gives the experimental error assumed in the calculation. The theoretical limit specified in the last column is the value of $\sigma(|g_e g_p|)$ for $\sigma_{ba}^{\mathrm{expt}} = 0$. The numbers within square brackets indicate multiplication by powers of 10.

Transition	$\sigma_{ba}^{\mathrm{expt}}$	$\sigma(|g_e g_p|)$	Theoretical limit
$1s_{1/2} - 2s_{1/2}$	15 Hz	1.7[−13]	1.7[−13]
$1s_{1/2} - 3s_{1/2}$	1 kHz	1.6[−13]	1.6[−13]
$1s_{1/2} - 20s_{1/2}$	1 kHz	1.5[−13]	1.5[−13]
$2s_{1/2} - 20s_{1/2}$	1 kHz	1.4[−13]	7.5[−14]
$2s_{1/2} - 20s_{1/2}$	100 Hz	7.6[−14]	7.5[−14]
$2s_{1/2} - 20s_{1/2}$	15 Hz	7.5[−14]	7.5[−14]
$8s_{1/2} - 20s_{1/2}$	100 Hz	2.1[−13]	2.1[−14]
$8s_{1/2} - 20s_{1/2}$	15 Hz	3.8[−14]	2.1[−14]
$8d_{5/2} - 20d_{5/2}$	100 Hz	2.1[−13]	2.8[−15]
$8d_{5/2} - 20d_{5/2}$	15 Hz	3.2[−14]	2.8[−15]
$3d_{5/2} - 20d_{5/2}$	1 kHz	2.6[−13]	2.8[−15]
$3d_{5/2} - 20d_{5/2}$	100 Hz	2.6[−14]	2.8[−15]

2. Numerical illustration

The potential reach of this approach in the low-mass region is indicated by the values of $\sigma(|g_e g_p|)$ presented in Table II. [Recall that this parameter determines the method's sensitivity to the effect of an NP interaction, with a lower value of $\sigma(|g_e g_p|)$ corresponding to a higher sensitivity.] The values of $\sigma_{ba}^{\mathrm{expt}}$ assumed in the calculation are hypothetical, with the exception of the entry for the $1s_{1/2} - 2s_{1/2}$ interval, which is the experimental uncertainty already achieved for this transition [43]. The rightmost column of the table gives the value of $\sigma(|g_e g_p|)$ calculated for $\sigma_{ba}^{\mathrm{expt}} = 0$. Values of $\sigma(|g_e g_p|)$ based on actual or hypothetical measurements of the isotope shift of the $1s_{1/2} - 2s_{1/2}$ and $1s_{1/2} - 3s_{1/2}$ transition frequencies are also presented in Fig. 6 over a wide range of mediator masses.

The first row of Table II and the black solid curves in the figure refer to the value of $\sigma(|g_e g_p|)$ based on the existing measurement of the isotope shift of the $1s_{1/2} - 2s_{1/2}$ interval [43]. This value is entirely consistent with the results of Fig. 5 and with the bounds calculated in Appendix C, which are based on the same data. The second row in the table and the green dash-dotted curves in Fig. 6 (almost indistinguishable from the black solid curves) refer to the value of $\sigma(|g_e g_p|)$ calculated from a hypothetical measurement of the isotope shift of the $1s_{1/2} - 3s_{1/2}$ interval, assuming an experimental uncertainty of 1 kHz on this quantity (for comparison, the error on the most recent determination of the $1s_{1/2} - 3s_{1/2}$ transition frequency in hydrogen is 0.72 kHz [35]). Although $\sigma_{ba}^{\mathrm{expt}}$ is considerably larger here, the resulting values of $\sigma(|g_e g_p|)$ are practically the same as those based on the $1s_{1/2} - 2s_{1/2}$ interval. The similarity between these two sets of results arises from the fact that σ_{ba}, the numerator of Eq. (30), is dominated by the nuclear size error for these transitions, which is roughly the same for the two intervals: In relative terms, the larger value of $\sigma_{ba}^{\mathrm{expt}}$ only produces a small increase in the value of σ_{ba}, which is largely compensated by an increase in the value of $\Delta \tilde{\nu}_{ba}^{\mathrm{NP}}$ ($\Delta \tilde{\nu}_{ba}^{\mathrm{NP}}$ is almost 20% larger for the $1s_{1/2}$-$3s_{1/2}$
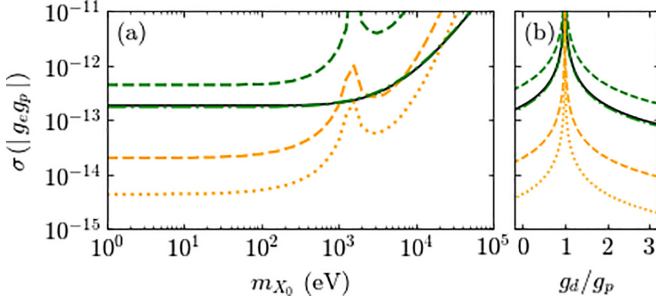
FIG. 6. Sensitivity parameter $\sigma(|g_e g_p|)$ for $g_\mu = g_e$ vs (a) m_{X_0}, assuming that $g_d/g_p = 2$, and (b) the ratio g_d/g_p, assuming that $m_{X_0} = 1$ eV. The black solid curves show results based on the existing data for the isotope shift of the $1s_{1/2} - 2s_{1/2}$ interval. The green dash-dotted curves (almost indistinguishable from the black solid curves) show results based on a hypothetical measurement of the isotope shift of the $1s_{1/2} - 3s_{1/2}$ interval with an experimental error of 1 kHz. The green dashed curves show the results which would be obtained by combining the isotope shift of the $1s_{1/2} - 2s_{1/2}$ interval with that of the $1s_{1/2} - 3s_{1/2}$ interval, assuming an experimental error of 1 kHz on the latter. The orange dashed curves show the results which would be obtained by combining the isotope shift of the $1s_{1/2} - 2s_{1/2}$ interval with that of the $2s_{1/2} - 20s_{1/2}$ interval, assuming an experimental error of 100 Hz on the latter. The orange dotted curves show the same as the orange dashed curves but for an experimental error of 15 Hz.

interval). Reducing the experimental uncertainties further would not improve the method's sensitivity for these two transitions. We note, however, that complementing the existing measurement of the $1s_{1/2}$-$3s_{1/2}$ transition frequency in hydrogen by a measurement of its isotope shift would be useful as an independent check of the results derived from the $1s_{1/2}$-$2s_{1/2}$ interval.

The scope for achieving a lower value of $\sigma(|g_e g_p|)$ within this approach can be inferred from the remaining rows of Table II. Using transitions between the ground state and more highly excited states would not lead to a significant gain in sensitivity without significantly reducing the uncertainties on the nuclear charge radii. Using transitions from the metastable $2s_{1/2}$ state to Rydberg states could lead to a twofold increase in sensitivity as long as the experimental error would not be much larger than 100 Hz (we have previously noted that reducing the experimental error to this level is likely to be achievable for such transitions [7]). Reaching higher sensitivities would require ultrahigh-precision isotope shift measurements on more highly excited states. As is explained in Appendix E, the theoretical limit of $\sigma(|g_e g_p|)$ is as small as 2.8×10^{-15} for transitions not involving s states, but approaching this limit would be particularly challenging experimentally. It is worth noting that the $3d_{3/2}$ and $3d_{5/2}$ states have a more significant NP shift than the other d states, which makes transitions from a $3d$ state to a Rydberg d state of particular interest in this context. As seen from the table, a sixfold reduction of $\sigma(|g_e g_p|)$ from its current best value could be achieved if the isotope shift of, e.g., the $3d_{5/2}$-$20d_{5/2}$ interval were measured with a precision of 100 Hz.

The other curves plotted in Fig. 6 refer to results obtained by combining two different isotope shifts in an approach described in the next section.

B. Bounds based on two isotope shifts

As noted in Sec. IV A, the sensitivity of the single-transition method is limited by the error on the nuclear size term when applied to transitions between s states. However, as we now discuss, this error can be eliminated by combining the isotope shifts of two different intervals.

Let us imagine that experimental values of the isotope shift would be known for two different transitions, say, for a transition from a state a to a state b and for a transition from a state c to a state d, all s states. Equations (27) and (28) give

$$g_e g_p \Delta \tilde{\nu}_{ba}^{\text{NP}} = \Delta \nu_{ba}^{\text{expt}} - \Delta \nu_{ba}^{\text{g}} - \Delta \nu_{ba}^{\text{ns}} - \Delta \nu_{ba}^{\text{oc}}, \quad (37)$$

$$g_e g_p \Delta \tilde{\nu}_{dc}^{\text{NP}} = \Delta \nu_{dc}^{\text{expt}} - \Delta \nu_{dc}^{\text{g}} - \Delta \nu_{dc}^{\text{ns}} - \Delta \nu_{dc}^{\text{oc}}. \quad (38)$$

(Recall that these equations refer to isotope shifts, not to transitions for a single isotope.) Let

$$\epsilon_1 = \frac{1}{n_a^3} - \frac{1}{n_b^3}, \quad \epsilon_2 = \frac{1}{n_c^3} - \frac{1}{n_d^3}. \quad (39)$$

In view of Eq. (22), multiplying Eq. (38) by ϵ_1/ϵ_2 and subtracting the product from Eq. (37) cancels the nuclear size terms. The result can be written as

$$g_e g_p = \frac{\Delta_{ba,dc}^{\text{expt}} - \Delta_{ba,dc}^{\text{g}} - \Delta_{ba,dc}^{\text{ns}} - \Delta_{ba,dc}^{\text{oc}}}{\tilde{\Delta}_{ba,dc}^{\text{NP}}}, \quad (40)$$

with

$$\Delta_{ba,dc}^{\text{expt}} = \Delta_{ba}^{\text{expt}} - (\epsilon_1/\epsilon_2)\Delta_{cd}^{\text{expt}}, \quad (41)$$

$$\Delta_{ba,dc}^{\text{g}} = \Delta_{ba}^{\text{g}} - (\epsilon_1/\epsilon_2)\Delta_{cd}^{\text{g}}, \quad (42)$$

$$\Delta_{ba,dc}^{\text{ns}} = \Delta_{ba}^{\text{ns}} - (\epsilon_1/\epsilon_2)\Delta_{cd}^{\text{ns}}, \quad (43)$$

$$\Delta_{ba,dc}^{\text{oc}} = \Delta_{ba}^{\text{oc}} - (\epsilon_1/\epsilon_2)\Delta_{cd}^{\text{oc}}, \quad (44)$$

and

$$\tilde{\Delta}_{ba,dc}^{\text{NP}} = \tilde{\Delta}_{ba}^{\text{NP}} - (\epsilon_1/\epsilon_2)\tilde{\Delta}_{cd}^{\text{NP}}. \quad (45)$$

We denote the uncertainties on $\Delta_{ba,dc}^{\text{expt}}$, $\Delta_{ba,dc}^{\text{g}}$, $\Delta_{ba,dc}^{\text{ns}}$, and $\Delta_{ba,dc}^{\text{oc}}$ by $\sigma_{ba,dc}^{\text{expt}}$, $\sigma_{ba,dc}^{\text{g}}$, $\sigma_{ba,dc}^{\text{ns}}$, and $\sigma_{ba,dc}^{\text{oc}}$, respectively. Assuming that the individual experimental errors $\sigma_{ba}^{\text{expt}}$ and $\sigma_{dc}^{\text{expt}}$ are uncorrelated,

$$\sigma_{ba,dc}^{\text{expt}} = \sqrt{\left(\sigma_{ba}^{\text{expt}}\right)^2 + \left(\epsilon_1 \sigma_{dc}^{\text{expt}}/\epsilon_2\right)^2}. \quad (46)$$

Given Eq. (34) and the fact that the error on the mass ratios contributes exactly in the same way for the two transitions,

$$\sigma_{ba,dc}^{\text{g}} = 0.10 \text{ kHz} \times \left[\frac{1}{n_a^2} - \frac{1}{n_b^2} - \frac{\epsilon_1}{\epsilon_2}\left(\frac{1}{n_d^2} - \frac{1}{n_c^2}\right)\right]. \quad (47)$$

By construction, $\Delta_{ba,dc}^{\text{ns}} = 0$. The errors on Δ_{ba}^{ns} and Δ_{dc}^{ns} being perfectly correlated, $\sigma_{ba,dc}^{\text{ns}}$ is also zero. Given how the different contributions to the Lamb shift scale with n, and in the current absence of a more in depth study of this issue, we

tentatively set

$$\sigma_{ba,dc}^{\mathrm{oc}} = 50 \text{ Hz}, \tag{48}$$

which is conservative. The 95% confidence interval of the value of $g_e g_p$ predicted by Eq. (40) is thus $\pm\sigma(|g_e g_p|)$, with

$$\sigma(|g_e g_p|) = 1.96 \frac{\sqrt{\left(\sigma_{ba,dc}^{\mathrm{expt}}\right)^2 + \left(\sigma_{ba,dc}^{\mathrm{g}}\right)^2 + \left(\sigma_{ba,dc}^{\mathrm{oc}}\right)^2}}{\left|\tilde{\Delta}_{ba,dc}^{\mathrm{NP}}\right|}. \tag{49}$$

Compared to Eq. (30), the numerator of Eq. (49) will typically be significantly smaller for transitions between s states. However, the NP shifts of the two intervals also partly cancel, and therefore the denominator of Eq. (49) may also be significantly smaller, offsetting the gain made by reducing the magnitude of the numerator. The result may be a reduction of sensitivity [a larger value of $\sigma(|g_e g_p|)$] compared to the single-transition method. For example, the value of $\sigma(|g_e g_p|)$ obtained by combining the existing results for the $1s_{1/2}$-$2s_{1/2}$ interval with the hypothetical results for the $1s_{1/2}$-$3s_{1/2}$ interval is higher than the values obtained from each of these intervals taken individually (the result of the combined calculation is represented by a green dashed curve in Fig. 6).

Nevertheless, a significant improvement in sensitivity on the single isotope shift method could be obtained by combining appropriately chosen intervals, provided the experimental uncertainties would be small enough. For example, the value of $\sigma(|g_e g_p|)$ based on the existing results for the $1s_{1/2} - 2s_{1/2}$ isotope shift would be reduced tenfold by combining these results with measurements of the $2s_{1/2} - 20s_{1/2}$ isotope shift if the latter was obtained with an experimental uncertainty of about 100 Hz (see the orange dashed curve in Fig. 6). Reducing this experimental uncertainty to 15 Hz would lower $\sigma(|g_e g_p|)$ to about 4.3×10^{-15} in the low-mass region (the orange dotted curve in Fig. 6), which is close to the limit set by the current uncertainties on the relevant QED corrections and nuclear masses (3.1×10^{-15} for this transition).

Finally, we should emphasize that the results presented in Fig. 6 depend on the value assumed for the ratio g_d/g_p, like those presented in Sec. III. The values of $\sigma(|g_e g_p|)$ given by Eqs. (30) and (49) are roughly proportional to $1/|g_d/g_p - 1|$. Setting $g_d = 2g_p$ leads to the results shown in Fig. 6(a). However, much larger values of $\sigma(|g_e g_p|)$ would be found for $g_d \approx g_p$, as shown by Fig. 6(b).

V. CONCLUSION

Precision transition measurements in deuterium and hydrogen are a direct way to tension well-motivated extensions of the standard model. The results presented in this article illustrate the advantages of combining results for these two isotopes when setting bounds on a new physics interaction that couples differently to a deuteron than to a proton.

Specifically, we have presented bounds based on the world spectroscopic hydrogen and deuterium data and bounds based only on the isotope shift of the $1s_{1/2}$-$2s_{1/2}$ interval. The former are more blunt than the latter for models in which $g_d \neq g_p$ (as defined above, g_d and g_p denote the coupling constants of the new physics interaction with a deuteron and a proton, respectively). However, they have the advantage of being based on

a number of independent measurements and a broad range of transitions. Their scope is limited by their well-known internal inconsistencies though. Resolving those would be of benefit in strengthening these bounds, besides reducing the uncertainties on the values of fundamental constants [29]. Where comparison is possible, our results are in broad agreement with those of Ref. [8], which were obtained independently and focus on specific theoretical models.

The bounds based on the isotope shift of the $1s_{1/2}$-$2s_{1/2}$ interval are more stringent [6]. As explained in Sec. IV, it would be useful to complement the existing measurements of the $1s_{1/2}$-$3s_{1/2}$ interval in hydrogen by measurements in deuterium at a similar level of precision so as to obtain bounds based on the isotope shift of this interval. Those bounds would provide a useful independent check on the results derived from the $1s_{1/2}$-$2s_{1/2}$ isotope shift. Measurements of that transition in deuterium at the required level of precision are currently considered [44].

The sensitivity of the isotope shift method for these two intervals is limited by the current uncertainties on the theory and the nuclear charge radii. We found that a measurement of the isotope shift of the $2s_{1/2}$-$20s_{1/2}$ interval (or more generally $2s_{1/2}$ to Rydberg s state) would make it possible to bypass this limitation, provided the experimental error would be sufficiently small, e.g., of the order of 0.1 kHz or better for the $2s_{1/2}$-$20s_{1/2}$ interval. As described above, theoretical errors can indeed be reduced by combining the isotope shift of such intervals and that of the $1s_{1/2}$-$2s_{1/2}$ interval, making the experimental error the main limitation of the method. Compared to the results based on currently available spectroscopic measurements, achieving an experimental uncertainty of 0.1 kHz would improve the sensitivity of the method by one order of magnitude in the low-mass region, for $g_d \neq g_p$.

These results and those of Ref. [8] thus suggest that any future precision experiments in hydrogenic atoms should consider whether the experimental method may be extended to deuterium as part of the planning stage.

APPENDIX A: IMPACT OF AN NP INTERACTION ON THE DETERMINATION OF r_p AND r_d IN MUONIC SPECIES

The nuclear charge radii derived from the experiments on muonic hydrogen and muonic deuterium were calculated from the respective Lamb shifts, which were themselves calculated from measured energy differences between hyperfine components of the $2s_{1/2}$ and $2p_{3/2}$ states [30,32]. In the following, we ascertain the maximal values of the coupling constants $g_\mu g_p$ and $g_\mu g_d$ for which a hypothetical NP shift of the $2s_{1/2} - 2p_{3/2}$ interval would have a negligible impact on these charge radii. We use atomic units throughout this Appendix, except where specified otherwise.

The NP shift in question reduces to $\delta E_{21}^{\text{NP}} - \delta E_{20}^{\text{NP}}$ in the nonrelativistic approximation, with $\delta E_{21}^{\text{NP}}$ and $\delta E_{20}^{\text{NP}}$ defined by Eq. (4). From Appendix B of [7],

$$\delta E_{21}^{\text{NP}} - \delta E_{20}^{\text{NP}} = \frac{B}{2m_{\text{r}}} \frac{C^2}{(C/m_{\text{r}} + 1)^4}, \quad \text{(A1)}$$

where m_{r} is the reduced mass of the system ($m_{\text{r}} \approx 186 m_e$ for muonic hydrogen and $m_{\text{r}} \approx 196 m_e$ for muonic deuterium). When $C \ll 1$, this shift is thus smaller by a factor m_e/m_{r} for the muonic species as compared to the electronic species. According to Eq. (A1), it also goes rapidly to zero for $C \to 0$, i.e., in the low-mass limit. However, this is so only because Eq. (A1) neglects relativistic effects and the spatial extension of the nucleus.[5]

Relativistic effects can be taken into account by replacing the radial wave functions $R_{nl}(r)$ by solutions of the Breit equation or the Dirac equation. We use Dirac wave functions and replace Eq. (4) by

$$\delta E_{n\kappa}^{\text{NP}} = \int_0^\infty [|P_{n\kappa}(r)|^2 + |Q_{n\kappa}(r)|^2] \frac{B \exp(-Cr)}{r} dr, \quad \text{(A2)}$$

where $P_{n\kappa}(r)$ and $Q_{n\kappa}(r)$ are the radial parts of the large and small components of the respective four-component spinor multiplied by r, and κ is the relativistic quantum number ($\kappa = -1$ for the $2s_{1/2}$ state, 1 for the $2p_{1/2}$ state, and -2 for the $2p_{3/2}$ state). The functions $P_{n\kappa}(r)$ and $Q_{n\kappa}(r)$ are calculated for a particle of mass μ moving in a central potential well $V(r)$ and are normalized according to the usual prescription,

$$\int_0^\infty [|P_{n\kappa}(r)|^2 + |Q_{n\kappa}(r)|^2] dr = 1. \quad \text{(A3)}$$

Setting $V(r) \equiv -1/r$ yields the Dirac wave functions of the respective hydrogenic states. However, choosing $V(r)$ in this way would involve neglecting vacuum polarization, which in muonic hydrogen and muonic deuterium accounts for a large part of the Lamb shift [46–48]. It would also involve neglecting the finite extension of its charge distribution, which can be expected to play a larger role here than in normal hydrogen since the wave functions of muonic species are more compact. It is therefore preferable to set

$$V(r) = V_{\text{Uehl}}(r) + V_N(r) \quad \text{(A4)}$$

when estimating the NP shift. Here $V_{\text{Uehl}}(r)$ is the Uehling potential, which accounts for the bulk of the vacuum polarization effects in muonic species [46], and $V_N(r)$ is the electrostatic muon-nucleus potential obtained in a model of the charge distribution of the latter. For convenience, we use a Gaussian model for this charge distribution, with an rms radius r_N equal to the experimental charge radius of either the proton or the deuteron. Thus

$$V_N(r) = -\frac{1}{r} \text{erf}(r/r_0), \quad \text{(A5)}$$

where $\text{erf}(\cdot)$ denotes the error function and $r_0 = (2/3)^{1/2} r_N$ [49,50]. The Uehling potential is calculated for this Gaussian

---

[5]Setting $V(r) \equiv -1/r$ gives the same value of $\langle 1/r \rangle$ in both the $2s_{1/2}$ and $2p_{1/2}$ states [45].

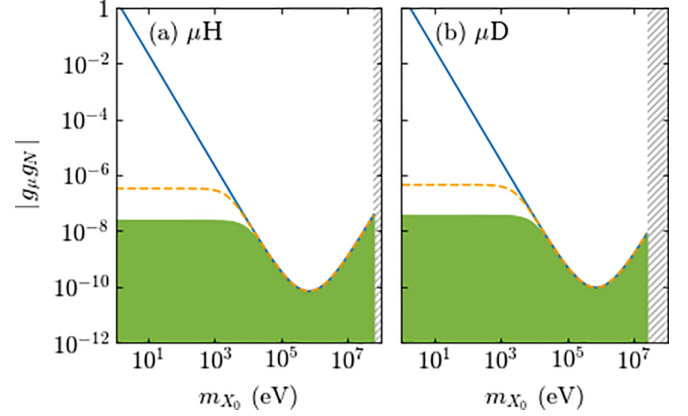
FIG. 7. Green areas show regions of the $(m_{X_0}, |g_\mu g_N|)$ plane in which an NP interaction between the muon and the nucleus would not shift the measured $2s_{1/2} - 2p_{3/2}$ interval by more than 5% of the experimental error on the respective Lamb shift in (a) muonic hydrogen ($g_N = g_p$) and (b) muonic deuterium ($g_N = g_d$). These regions would be predicted to extend upward to the orange dashed curves if vacuum polarization and the finite size of the nucleus were ignored or to the blue solid curves in the nonrelativistic approximation for a point nucleus. We do not present results for the ranges of values of m_{X_0} indicated by the shaded regions in view of the uncertainty on the form of the NP interaction within the nucleus.

charge distribution rather than for a point nuclear charge, and both $V_N(r)$ and $V_{\text{Uehl}}(r)$ are taken into account to all orders by solving the Dirac equation nonperturbatively. The approach follows Ref. [50]. We used the program QEDMOD [51] for calculating the Uehling potential and the program RADIAL [52] for integrating the Dirac equation.

As mentioned at the beginning of this Appendix, we want to ascertain how strong an NP interaction could be without significantly affecting the nuclear charge radii derived from the muonic data. We define an upper bound on $|g_\mu g_N|$, $|g_\mu g_N|_{\text{max}}$, such that the effect of an NP interaction would be negligible if $|g_\mu g_N| < |g_\mu g_N|_{\text{max}}$ but might be significant if $|g_\mu g_N| \gtrsim |g_\mu g_N|_{\text{max}}$. Conservatively, we take $|g_\mu g_N|_{\text{max}}$ to be the value of $|g_\mu g_N|$ at which the NP shift of the $2s_{1/2} - 2p_{3/2}$ interval is 5% of the error on the experimental Lamb shift, i.e., 0.12 μeV in muonic hydrogen (μH) and 0.17 μeV in muonic deuterium (μD).

The region of the $(m_{X_0}, |g_\mu g_N|)$ plane in which a hypothetical NP interaction would be negligible according to this definition is identified by the green areas in Fig. 7. We assume no definite relationship between $g_\mu g_N$ for μH and $g_\mu g_N$ for μD. We stress that these green areas only indicate the region of the parameter space in which an NP shift would not matter for the deduction of the proton or deuteron radius; they do not indicate whether a hypothetical NP interaction might or might not be compatible with existing data. Given the uncertainty on the form of the NP interaction inside the nucleus, we do not venture predictions of the importance of an NP shift for a mediator mass large enough that the region $r \lesssim 2r_N$ contributes significantly to the integral in Eq. (A2). This mass region starts at about 70 MeV for muonic hydrogen and about 30 MeV for muonic deuterium. The corresponding regions of Fig. 7 are shaded to indicate that they are not considered in the present analysis.

Figure 7(a) shows that $|g_\mu g_N|_{\max}$ does not much exceed 1×10^{-8} for $m_{X_0} < 10$ keV. The data for electronic hydrogen exclude the possibility that $|g_e g_p|$ could be as large as 1×10^{-8} between 1 eV and 10 keV [see, e.g., Figs. 1(a) and 1(b)]. Assuming that lepton universality still holds true for the coupling with an NP interaction, so that $g_\mu = g_e$, we can thus conclude that an NP interaction would have but a negligible impact on the values of r_p in this mass range. Given the results of Figs. 1(c) and 1(d), the same also applies to the determination of r_d from the measurements in muonic deuterium, at least for carrier masses between 10 eV and 10 keV. However, the bounds based on the spectroscopy of electronic hydrogen and electronic deuterium do not clearly exclude the possibility of a significant NP interaction with carrier mass well above 10 keV.

It is worth noting the importance of $V_{\mathrm{Uehl}}(r)$ and $V_N(r)$ in this context. Indeed, setting $V(r) = -1/r$ yields the result indicated by orange dashed curves in Figs. 7(a) and 7(b). As seen from these figures, $|g_\mu g_N|_{\max}$ is somewhat overestimated in the low-mass region, within this approximation.

The value of $|g_\mu g_N|_{\max}$ derived from Eq. (A1) is also shown in Fig. 7 (the blue solid curves): As is readily seen, the nonrelativistic approximation is good for $m_{X_0} > 10$ keV and unsuitable for $m_{X_0} < 10$ keV.

APPENDIX B: NOTES ABOUT THE CALCULATIONS

The results presented in this paper are largely based on the set of 29 measured transition energies between states of electronic hydrogen and electronic deuterium used by CODATA in their most recent determination of the Rydberg constant [29]. This set is listed in Table X of that reference, as the input data A1–A29. The set of data used in the present work differs in the following ways.

(i) We also use the recent measurements of the $1s_{1/2} - 3s_{1/2}$ and $2s_{1/2} - 8d_{5/2}$ transition energies in electronic hydrogen [35,36], as well as the experimental results quoted in Ref. [53] for transitions between high circular states of electronic hydrogen [specifically, and as explained in [7], we derive an experimental energy for the transition between the $(n = 27, l = 26)$ and $(n = 28, l = 27)$ states from the value of $\mathcal{R}$ obtained in that work].

(ii) For the input datum A28 (the $2s_{1/2} - 2p_{1/2}$ Lamb shift measurement of Ref. [54]), we use the value recently recommended in Ref. [55] rather than the original value.

(iii) We exclude the input datum A7 (the 2013 measurement of the $1s_{1/2}$-$2s_{1/2}$ transition energy in electronic hydrogen [56]), in view of its strong correlation with the input datum A6 (the 2011 measurement of that transition). This strong correlation tends to inflate the value of χ^2 significantly in fits using both values. When used individually, the resulting confidence levels are practically indistinguishable. However, they tend to decrease significantly when both these transition energies are included in the fit. The difficulty does not arise for the other intervals for which several different experimental values are included in the data set, as in these other cases the experimental errors are not strongly correlated with each other.

(iv) We use the input datum A5 (the isotope shift of the $1s_{1/2}$-$2s_{1/2}$ interval in electronic hydrogen [43]) as an independent input to the χ^2 fit only when combining hydrogen and deuterium data. We do not use this datum at all in calculations of bounds based only in measurements in hydrogen. For bounds based only in measurements in deuterium, we use it in conjunction with the input datum A6 to generate an experimental value for the $1s_{1/2}$-$2s_{1/2}$ transition frequency in deuterium [57], which is used in the fit.

The experimental data for the muonic species are the Lamb shifts measured by the CREMA Collaboration [30,32]. The correlation coefficients used in the χ^2 fitting are taken from Ref. [29] (the errors on the experimental results not considered in that reference can safely be assumed to be uncorrelated with those considered in it and with each other). No magnification of the experimental uncertainties was made for producing the results shown in Figs. 1, 2, and 5 and the results represented by the brown curves in Fig. 4. The experimental uncertainties were increased by 60% for producing the results shown in Fig. 3 and those represented by the black curves in Fig. 4.

The standard model calculations follow Appendix C of [7] for the electronic species and, except where specified otherwise, Refs. [30,31] for the muonic species. We stress that we take the finite size of the nucleus into account for both the electronic and the muonic species, which is important for the accuracy of the models.

APPENDIX C: ISOTOPE SHIFT ANALYSIS WITH AN NP INTERACTION

As discussed in Sec. III C and in previous work [6], tight bounds on the NP coupling constants can be derived from the measurements of the $1s_{1/2} - 2s_{1/2}$ interval in electronic hydrogen and deuterium, in conjunction with the measurements on the nuclear radius in muonic hydrogen and deuterium. The calculations reported in Sec. III C follow a general approach applicable to any number of transitions. However, they do not make use of particularly precise theoretical results, reported in Refs. [40,41], which are specific to the isotope shift of that interval. An alternative approach to obtaining bounds on an NP interaction, taking advantage of these theoretical results, is outlined in this Appendix.

The key experimental evidence is the difference $\Delta \nu^{\mathrm{expt}}$ between the $1s_{1/2}$-$2s_{1/2}$ transition frequency of electronic deuterium and that of electronic hydrogen [43]:

$$\Delta \nu^{\mathrm{expt}} = \Delta \nu^{\mathrm{expt}}_{2s1s,e\mathrm{D}} - \Delta \nu^{\mathrm{expt}}_{2s1s,e\mathrm{H}}$$
$$= 670\,994\,334.606(15)\ \mathrm{kHz}. \tag{C1}$$

Allowing for a hypothetical NP interaction, the theoretical isotope shift is $\Delta \nu^{\mathrm{SM}} + \Delta \nu^{\mathrm{NP}}$, where $\Delta \nu^{\mathrm{SM}}$ is the isotope shift calculated within the standard model and $\Delta \nu^{\mathrm{SM}}$ is a new physics correction. In terms of the NP shifts defined by Eq. (8),

$$\Delta \nu^{\mathrm{NP}} = \Delta \nu^{\mathrm{NP}}_{2s1s,e\mathrm{D}} - \Delta \nu^{\mathrm{NP}}_{2s1s,e\mathrm{H}}. \tag{C2}$$

Moreover [41],

$$\Delta\nu^{\mathrm{SM}} = \Delta\nu^{\mathrm{SM}}_{2s1s,eD} - \Delta\nu^{\mathrm{SM}}_{2s1s,eH}$$

$$= 670\,999\,567.88(42)\text{ kHz}$$

$$- \frac{7\alpha^4 m_e c^2}{12 h \hbar_{\mathrm{C}}^2}\left[\left(\frac{m_{\mathrm{r}}^{eD}}{m_e}\right)^3 r_d^2 - \left(\frac{m_{\mathrm{r}}^{eH}}{m_e}\right)^3 r_p^2\right], \quad \text{(C3)}$$

where h is Planck's constant, α is the fine-structure constant, and $\hbar_{\mathrm{C}}$ is the reduced Compton wavelength. Equating $\Delta\nu^{\mathrm{SM}} + \Delta\nu^{\mathrm{NP}}$ to $\Delta\nu^{\mathrm{expt}}$ and rearranging yields the equation $\Delta = 0$, where

$$\Delta = 5233.27(42)\text{ kHz} + \Delta\nu^{\mathrm{NP}}$$

$$- \frac{7\alpha^4 m_e c^2}{12 h \hbar_{\mathrm{C}}^2}\left[\left(\frac{m_{\mathrm{r}}^{eD}}{m_e}\right)^3 r_d^2 - \left(\frac{m_{\mathrm{r}}^{eH}}{m_e}\right)^3 r_p^2\right], \quad \text{(C4)}$$

with the nuclear charge radii obtained from the measurements in muonic hydrogen and muonic deuterium. For any given values of g_p, g_d, g_e, and g_μ, Δ is known only within a certain error σ arising primarily from the experimental and theoretical errors on $\Delta\nu^{\mathrm{expt}}$, $\Delta\nu^{\mathrm{NP}}$, r_p, and r_d. For given values of the ratio g_d/g_p, of the ratio g_μ/g_e, and of the mass m_{X_0}, setting

$$|\Delta| = 1.96\sigma \quad \text{(C5)}$$

then yields the value of $g_e g_p$ beyond which the possibility of an NP interaction is excluded at the 95% confidence level.

The bounds generated in this way are in close agreement with the "isotope shift" results of Figs. 4 and 5. The respective bounds on $g_e g_p$ differ by at most 3% in the mass range spanned by these figures.

It should be noted that this approach is useful only for cases where $g_d/g_p \neq 1$, as for $g_d = g_p$ the new physics correction term $\Delta\nu^{\mathrm{NP}}$ is proportional to $g_e g_p \times (m_{\mathrm{r}}^{eD} - m_{\mathrm{r}}^{eH})/m_e$ rather than to $g_e g_p$. For $r = 1$, Eq. (C5) yields bounds on $g_e g_p$ well above the values excluded, e.g., by the results of Figs. 1(e) and 1(f).

APPENDIX D: FURTHER RESULTS

1. World data with reduced error magnification

Distributions of confidence levels obtained without or with an error magnification of 20% are shown in Fig. 8, for comparison with Fig. 3(b) (for which the error magnification is 60%). Figures 8(a) and 8(b) both refer to a repulsive interaction with $r = 1$, like Fig. 3(b).

2. Other muonic deuterium models

Figure 9 shows the results obtained for a repulsive NP interaction with $r = 2$ when muonic deuterium is described as per Ref. [32] or Ref. [39], rather than as per the more recent theory of Ref. [31] as we do in Fig. 5. A comparison of these results to Fig. 5(b) illustrates the sensitivity of these confidence levels on the details of small QED corrections. In particular, Fig. 9(a) excludes the possibility of an attractive NP interaction and strongly points towards the existence of a repulsive NP interaction, whereas Figs. 9(b) and 5(b) do not.
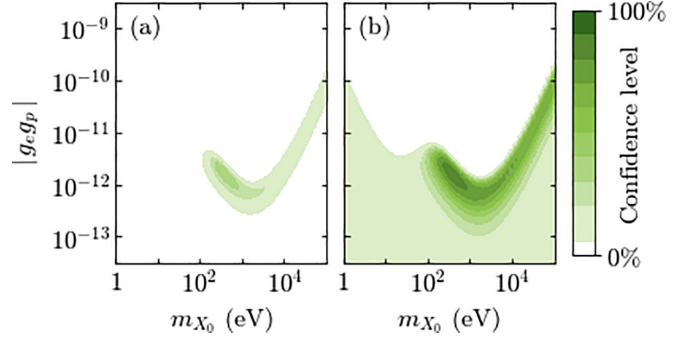

FIG. 8. Confidence level that a repulsive NP interaction is compatible with the world spectroscopic data for electronic hydrogen, electronic deuterium, muonic hydrogen, and muonic deuterium, assuming that $g_d = g_p$ and $g_\mu = g_e$. (a) Results obtained without magnification of the experimental uncertainties. (b) Results obtained when the experimental uncertainties are increased by 20%. As in Fig. 1, the possibility of an NP interaction with parameters falling in a white region is excluded at the 95% confidence level.

APPENDIX E: COMMENT ON THE SENSITIVITY OF THE ISOTOPE SHIFT METHOD IN THE LOW-MASS LIMIT

The right-hand side of Eq. (30) reduces to a simpler form in the low-mass limit as the denominator can be worked out in full generality when $m_{X_0} = 0$. Indeed, the NP interaction potential V_{NP} tends to a $1/r$ potential in that limit, which makes it possible to use the virial theorem to calculate the NP shifts $\delta E_{nl}^{\mathrm{NP}}$. The result reads

$$\Delta\tilde{\nu}_{ba}^{\mathrm{NP}} \approx \frac{8\pi\epsilon_0}{e^2} B \mathcal{R}\left[r\frac{m_{\mathrm{r}}^{eD}}{m_e} - \frac{m_{\mathrm{r}}^{eH}}{m_e}\right]\left(\frac{1}{n_a^2} - \frac{1}{n_b^2}\right). \quad \text{(E1)}$$
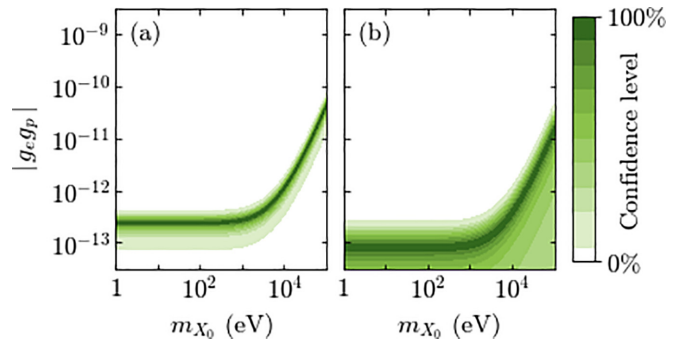

FIG. 9. Confidence level that a repulsive NP interaction is compatible with the $1s_{1/2} - 2s_{1/2}$ transition frequency measured in electronic hydrogen and electronic deuterium and with the nuclear charge radii derived from measurements in muonic hydrogen and muonic deuterium, assuming that $g_d = 2g_p$ and $g_\mu = g_e$. (a) Results obtained when the muonic deuterium structure is described as per Ref. [32]. (b) Results obtained when the muonic deuterium structure is described as per Ref. [39]. As in Fig. 1, the possibility of an NP interaction with parameters falling in a white region is excluded at the 95% confidence level.

Thus $\Delta\tilde{\nu}_{ba}^{\mathrm{NP}}$ has the same dependence on n_a and n_b as σ_{ba}^{g}, in this limit. Moreover, the numerator reduces to

$$1.96\sqrt{\left(\sigma_{ba}^{\mathrm{expt}}\right)^2 + \left(\sigma_{ba}^{\mathrm{g}}\right)^2}$$

in the case of transitions between non-s states, since $\sigma_{ba}^{\mathrm{ns}} = \sigma_{ba}^{\mathrm{oc}} = 0$ for such transitions. This quantity cannot be lower than $1.96\sigma_{ba}^{\mathrm{g}}$. The upshot is that for low values of m_{X_0}, $\sigma(|g_e g_p|)$ cannot be lower than

$$\frac{1.96 \times 0.10 \text{ kHz}}{(8\pi\epsilon_0 B\mathcal{R}/e^2)\left[rm_{\mathrm{r}}^{e\mathrm{D}}/m_e - m_{\mathrm{r}}^{e\mathrm{H}}/m_e\right]}$$

for transitions between d states, which for $r = 2$ is 2.8×10^{-15} (a value set by the current uncertainty on the proton and the deuteron masses).

---

[1] J. Jaeckel and S. Roy, Spectroscopy as a test of Coulomb's law: A probe of the hidden sector, Phys. Rev. D **82**, 125020 (2010).

[2] S. G. Karshenboim, Precision physics of simple atoms and constraints on a light boson with ultraweak coupling, Phys. Rev. Lett. **104**, 220406 (2010).

[3] S. G. Karshenboim, Constraints on a long-range spin-independent interaction from precision atomic physics, Phys. Rev. D **82**, 073003 (2010).

[4] P. Brax and C. Burrage, Atomic precision tests and light scalar couplings, Phys. Rev. D **83**, 035020 (2011).

[5] P. Brax and C. Burrage, Explaining the proton radius puzzle with disformal scalars, Phys. Rev. D **91**, 043515 (2015).

[6] C. Delaunay, C. Frugiuele, E. Fuchs, and Y. Soreq, Probing new spin-independent interactions through precision spectroscopy in atoms with few electrons, Phys. Rev. D **96**, 115002 (2017).

[7] M. P. A. Jones, R. M. Potvliege, and M. Spannowsky, Probing new physics using Rydberg states of atomic hydrogen, Phys. Rev. Res. **2**, 013244 (2020).

[8] C. Delaunay, J.-P. Karr, T. Kitahara, J. C. J. Koelemeij, Y. Soreq, and J. Zupan, Self-consistent extraction of spectroscopic bounds on light new physics, Phys. Rev. Lett. **130**, 121801 (2023).

[9] M. S. Safronova, D. Budker, D. DeMille, D. F. Jackson Kimball, A. Derevianko, and C. W. Clark, Search for new physics with atoms and molecules, Rev. Mod. Phys. **90**, 025008 (2018).

[10] C. Delaunay, R. Ozeri, G. Perez, and Y. Soreq, Probing atomic Higgs-like forces at the precision frontier, Phys. Rev. D **96**, 093001 (2017).

[11] J. C. Berengut, D. Budker, C. Delaunay, V. V. Flambaum, C. Frugiuele, E. Fuchs, C. Grojean, R. Harnik, R. Ozeri, G. Perez, and Y. Soreq, Probing new long-range interactions by isotope shift spectroscopy, Phys. Rev. Lett. **120**, 091801 (2018).

[12] B. Ohayon, H. Rhangdale, A. J. Geddes, J. C. Berengut, and G. Ron, Isotope shifts in ^{20,22}Ne: Precision measurements and global analysis in the framework of intermediate coupling, Phys. Rev. A **99**, 042503 (2019).

[13] I. Counts, J. Hur, D. P. L. Aude Craik, H. Jeon, C. Leung, J. C. Berengut, A. Geddes, A. Kawasaki, and V. Vuletić, Evidence for nonlinear isotope shift in Yb$^+$ search for new boson, Phys. Rev. Lett. **125**, 123002 (2020).

[14] C. Solaro, S. Meyer, K. Fisher, J. C. Berengut, E. Fuchs, and M. Drewsen, Improved isotope-shift-based bounds on bosons beyond the standard model through measurements of the $^2D_{3/2} - ^2D_{5/2}$ interval in Ca$^+$, Phys. Rev. Lett. **125**, 123003 (2020).

[15] J. Hur, D. P. L. Aude Craik, I. Counts, E. Knyazev, L. Caldwell, C. Leung, S. Pandey, J. C. Berengut, A. Geddes, W. Nazarewicz *et al.*, Evidence of two-source King plot nonlinearity in spec-

troscopic search for new boson, Phys. Rev. Lett. **128**, 163201 (2022).

[16] N.-H. Rehbehn, M. K. Rosner, J. C. Berengut, P. O. Schmidt, T. Pfeifer, M. F. Gu, and J. R. Crepo López-Urrutia, Narrow and ultranarrow transitions in highly charged Xe ions as probes of fifth forces, Phys. Rev. Lett. **131**, 161803 (2023).

[17] A. V. Viatkina, V. A. Yerokhin, and A. Surzhykov, Calculation of isotope shifts and King-plot nonlinearities in Ca$^+$, Phys. Rev. A **108**, 022802 (2023).

[18] S. O. Allehabi, V. A. Dzuba, V. V. Flambaum, and A. V. Afanasjev, Nuclear deformation as a source of the nonlinearity of the King plot in the Yb$^+$ ion, Phys. Rev. A **103**, L030801 (2021).

[19] R. A. Müller, V. A. Yerokhin, A. N. Artemyev, and A. Surzhykov, Nonlinearities of King's plot and their dependence on nuclear radii, Phys. Rev. A **104**, L020802 (2021).

[20] P. Munro-Laylim, V. A. Dzuba, and V. V. Flambaum, Nuclear polarization and the contributions of relativistic effects to King plot nonlinearity, Phys. Rev. A **105**, 042814 (2022).

[21] A. J. Krasznahorkay, M. Csatlós, L. Csige, Z. Gácsi, J. Gulyás, M. Hunyadi, I. Kuti, B. M. Nyakó, L. Stuhl, J. Timár, T. G. Tornyi, Z. Vajta, T. J. Ketel, and A. Krasznahorkay, Observation of anomalous internal pair creation in ^{8}Be: A possible indication of a light, neutral boson, Phys. Rev. Lett. **116**, 042501 (2016).

[22] A. J. Krasznahorkay, M. Csatlós, L. Csige, Z. Gácsi, J. Gulyás, Á. Nagy, N. Sas, J. Timár, T. G. Tornyi, I. Vajda, and A. Krasznahorkay, New results on the ^{8}Be anomaly, J. Phys.: Conf. Ser. **1056**, 012028 (2018).

[23] J. L. Feng, B. Fornal, I. Galon, S. Gardner, J. Smolinsky, T. M. P. Tait, and P. Tanedo, Particle physics models for the 17 MeV anomaly in beryllium nuclear decays, Phys. Rev. D **95**, 035017 (2017).

[24] D. Barducci and C. Toni, An updated view on the ATOMKI nuclear anomalies, J. High Energy Phys. 06 (2022) 077.

[25] D. Alves (LHC New Physics Working Group), Simplified models for LHC new physics searches, J. Phys. G **39**, 105005 (2012).

[26] K. Y. Khabarova and N. N. Kolachevsky, Proton charge radius, Usp. Fiz. Nauk **191**, 1095 (2021). [Phys. Usp. **64**, 1038 (2021)].

[27] P. J. Mohr, D. B. Newell, and B. N. Taylor, CODATA recommended values of the fundamental physical constants: 2014, Rev. Mod. Phys. **88**, 035009 (2016).

[28] V. A. Yerokhin, K. Pachucki, and V. Patkóš, Theory of the Lamb shift in hydrogen and light hydrogen-like ions, Ann. Phys. (Berlin) **531**, 1800324 (2019).

[29] E. Tiesinga, P. J. Mohr, D. B. Newell, and B. N. Taylor, CODATA recommended values of the fundamental physical constants: 2018, Rev. Mod. Phys. **93**, 025010 (2021).

[30] A. Antognini, F. Nez, K. Schuhmann, F. D. Amaro, F. Biraben, J. M. R. Cardoso, D. S. Covita, A. Dax, S. Dhawan, M. Diepold *et al.*, Proton structure from the measurement of 2S-2P transition frequencies of muonic hydrogen, Science **339**, 417 (2013).

[31] V. Lensky, F. Hagelstein, and V. Pascalutsa, A reassessment of nuclear effects in muonic deuterium using pionless effective field theory at N3LO, Phys. Lett. B **835**, 137500 (2022).

[32] R. Pohl, F. Nez, L. M. P. Fernandes, F. D. Amaro, F. Biraben, J. M. R. Cardoso, D. S. Covita, A. Dax, S. Dhawan, M. Diepold *et al.*, Laser spectroscopy of muonic deuterium, Science **353**, 669 (2016).

[33] P. J. Mohr and B. N. Taylor, CODATA recommended values of the fundamental physical constants: 1998, Rev. Mod. Phys. **72**, 351 (2000).

[34] N. Bezginov, T. Valdez, M. Horbatsch, A. Marsman, A. C. Vutha, and E. A. Hessels, A measurement of the atomic hydrogen Lamb shift and the proton charge radius, Science **365**, 1007 (2019).

[35] A. Grinin, A. Matveev, D. C. Yost, L. Maisenbacher, V. Wirth, R. Pohl, T. W. Hänsch, and T. Udem, Two-photon frequency comb spectroscopy of atomic hydrogen, Science **370**, 1061 (2020).

[36] A. D. Brandt, S. F. Cooper, C. Rasor, Z. Burkley, A. Matveev, and D. C. Yost, Measurement of the $2S_{1/2}$–$8D_{5/2}$ transition in hydrogen, Phys. Rev. Lett. **128**, 023001 (2022).

[37] J. C. Bernauer, The proton radius puzzle — 9 years later, EPJ Web Conf. **234**, 01001 (2020).

[38] C. Delaunay (private communication).

[39] M. Kalinowski, Deuteron charge radius from the Lamb-shift measurement in muonic deuterium, Phys. Rev. A **99**, 030501(R) (2019).

[40] U. D. Jentschura, A. Matveev, C. G. Parthey, J. Alnis, R. Pohl, T. Udem, N. Kolachevsky, and T. W. Hänsch, Hydrogen-deuterium isotope shift: From the 1S-2S-transition frequency to the proton-deuteron charge-radius difference, Phys. Rev. A **83**, 042505 (2011).

[41] K. Pachucki, V. Patkóš, and V. A. Yerokhin, Three-photon-exchange nuclear structure correction in hydrogenic systems, Phys. Rev. A **97**, 062511 (2018).

[42] F. Heiße, F. Köhler-Langes, S. Rau, J. Hou, S. Junck, A. Kracke, A. Mooser, W. Quint, S. Ulmer, G. Werth *et al.*, High-precision measurement of the proton's atomic mass, Phys. Rev. Lett. **119**, 033001 (2017).

[43] C. G. Parthey, A. Matveev, J. Alnis, R. Pohl, T. Udem, U. D. Jentschura, N. Kolachevsky, and T. W. Hänsch, Precision measurement of the hydrogen-deuterium 1S-2S isotope shift, Phys. Rev. Lett. **104**, 233001 (2010).

[44] P. Yzombard, S. Thomas, L. Julien, F. Biraben, and F. Nez, 1S-3S cw spectroscopy of hydrogen/deuterium atom, Eur. Phys. J. D **77**, 23 (2023).

[45] V. M. Burke and I. P. Grant, The effect of relativity on atomic wave functions, Proc. Phys. Soc. **90**, 297 (1967); S. K. Suslov, Expectation values in relativistic Coulomb problems, J. Phys. B **42**, 185003 (2009).

[46] E. Borie and G. A. Rinker, The energy levels of muonic atoms, Rev. Mod. Phys. **54**, 67 (1982).

[47] A. Antognini, F. Kottmann, F. Biraben, P. Indelicato, F. Nez, and R. Pohl, Theory of the 2S-2P Lamb shift and 2S hyperfine splitting in muonic hydrogen, Ann. Phys. (NY) **331**, 127 (2013).

[48] J. J. Krauth, M. Diepold, B. Franke, A. Antognini, F. Kottmann, and R. Pohl, Theory of the $n = 2$ levels in muonic deuterium, Ann. Phys. (NY) **366**, 168 (2016).

[49] J. L. Friar, Nuclear finite-size effects in light muonic atoms, Ann. Phys. (NY) **122**, 151 (1979).

[50] P. Indelicato, Nonperturbative evaluation of some QED contributions to the muonic hydrogen $n = 2$ Lamb shift and hyperfine structure, Phys. Rev. A **87**, 022501 (2013).

[51] V. M. Shabaev, I. I. Tupitsyn and V. A. Yerokhin, QEDMOD: Fortran program for calculating the model Lamb-shift operator, Comput. Phys. Commun. **223**, 69 (2018).

[52] F. Salvat and J. M. Fernández-Varea, RADIAL: A Fortran subroutine package for the solution of the radial Schrödinger and Dirac wave equations, Comput. Phys. Commun. **240**, 165 (2019).

[53] J. C. De Vries, A precision millimeter-wave measurement of the Rydberg frequency, Ph.D. thesis, MIT, 2002.

[54] S. R. Lundeen and F. M. Pipkin, Measurement of the Lamb shift in hydrogen, $n = 2$, Phys. Rev. Lett. **46**, 232 (1981).

[55] A. Marsman, M. Horbatsch, Z. A. Corriveau, and E. A. Hessels, Systematic effects important to separated-oscillator-field measurements of the $n = 2$ Lamb shift in atomic hydrogen, Phys. Rev. A **98**, 012509 (2018).

[56] A. Matveev, C. G. Parthey, K. Predehl, J. Alnis, A. Beyer, R. Holzwarth, T. Udem, T. Wilken, N. Kolachevsky, M. Abgrall *et al.*, Precision measurement of the hydrogen 1S-2S frequency via a 920-km fiber link, Phys. Rev. Lett. **110**, 230801 (2013).

[57] R. Pohl, F. Nez, T. Udem, A. Antognini, A. Beyer, H. Fleurbaey, A. Grinin, T. W. Hänsch, L. Julien, F. Kottmann *et al.*, Deuteron charge radius and Rydberg constant from spectroscopy data in atomic deuterium, Metrologia **54**, L1 (2017).